ORNL-3407
UC-34 – Physics
TID-4500 (19th ed.)

EXPERIMENTAL DETERMINATION OF CORRECTIONS TO THE NEUTRON ACTIVATION OF GOLD FOILS EXPOSED IN WATER

W. Zobel

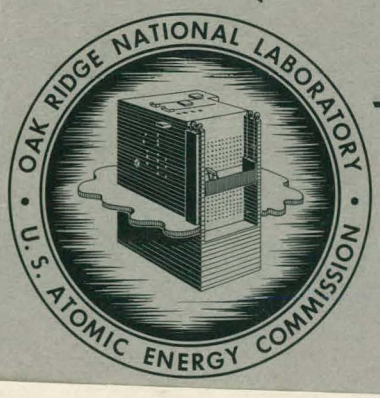

OAK RIDGE NATIONAL LABORATORY
operated by
UNION CARBIDE CORPORATION
for the
U.S. ATOMIC ENERGY COMMISSION

DISCLAIMER

ORNL-3407

Contract No. W-7405-eng-26

Neutron Physics Division

EXPERIMENTAL DETERMINATION OF CORRECTIONS TO THE NEUTRON ACTIVATION OF GOLD FOILS EXPOSED IN WATER

W. Zobel

Date Issued

APR 4 - 1963

OAK RIDGE NATIONAL LABORATORY
Oak Ridge, Tennessee
operated by
UNION CARBIDE CORPORATION
for the
U.S. ATOMIC ENERGY COMMISSION

THIS PAGE

WAS INTENTIONALLY

LEFT BLANK

ABSTRACT

The corrections required to deduce unperturbed neutron fluxes from measurements with foil absorbers have been determined experimentally for the case of gold foils exposed in a light-water medium. The results are in good agreement with the theoretical predictions of Dalton and Osborn and of Ritchie and Eldridge.

THIS PAGE

WAS INTENTIONALLY

LEFT BLANK

TABLE OF CONTENTS

INTRODUCTION

One of the common methods for determining the neutron flux in a given medium is based on the beta or gamma-ray activity induced by the neutrons in a foil of suitable material. This material should be easily available and should have a high absorption cross section in the energy range of interest; the half-life of the resulting activity should be neither so short that most of the activity disappears prior to counting nor so long that the foil cannot be activated to saturation, if required, in a reasonable length of time. Indium and gold are materials that meet these criteria well and are in wide use in the measurement of low-energy neutron fluxes.[1]

With gold foils, the thermal-neutron flux in a medium is determined by exposing bare foils and cadmium-covered foils at the same location and calculating the flux from the difference of the activities produced. This cadmium-difference activity cannot be used directly, however, but must be corrected for the various effects which tend to give a false reading. These include the depression of the flux due to the presence of an absorber in the neutron field; the self-shielding in the foil, resulting in the activation at points within the foil being lower than at its surface; the self-absorption in the foil of the radiation emitted by the activated nuclei;

1. It should here be stated that, of course, a thin $\frac{1}{v}$ absorber measures neutron density, which may then be converted to flux by multiplying by the appropriate average neutron velocity; for the sake of convenience this distinction is not made in this report.

and the absorption of neutrons with energies above the cadmium cut-off by the cadmium covers. The work reported here is the determination of the corrections applicable to gold foils exposed in a water medium, for which the activation is determined by gamma-ray counting techniques. Foils 1 cm square, varying in thickness from ~0.040 mg/cm^2 to ~500 mg/cm^2, and circular foils, having diameters of 0.5, 1, 2, and 3 cm and varying in thickness from 0.001 in. to 0.010 in., were exposed in an isotropic thermal neutron flux. Similar square foils, ~1 mg/cm^2 to ~500 mg/cm^2 thick, were also activated at a location where the flux was decreasing with a relaxation length λ = 5.8 cm.

Studies similar to the present one were performed previously (1-7). The closest similarity is with the work of de Troyer and Tavernier (2), who, however, considered only circular foils of 2.5 cm diameter and a minimum foil thickness of 0.001 in. For practical purposes it became important to consider foils of other than circular shape, as well as circular foils with a range of diameters. It also appeared desirable to use thinner foils.

EXPERIMENTAL ARRANGEMENT

The experiment was carried out in the configuration tank of the ORNL Lid Tank Shielding Facility (8). The configuration tank is shown installed in Fig. 1. The radiation source, a 20.3%-enriched-uranium disk 28 in. in diameter, is located on the other side of the (aluminum) window. The foils used in the experiment were attached to a long Lucite foil holder, Fig. 2, suspended from the instrument carriage in place of the

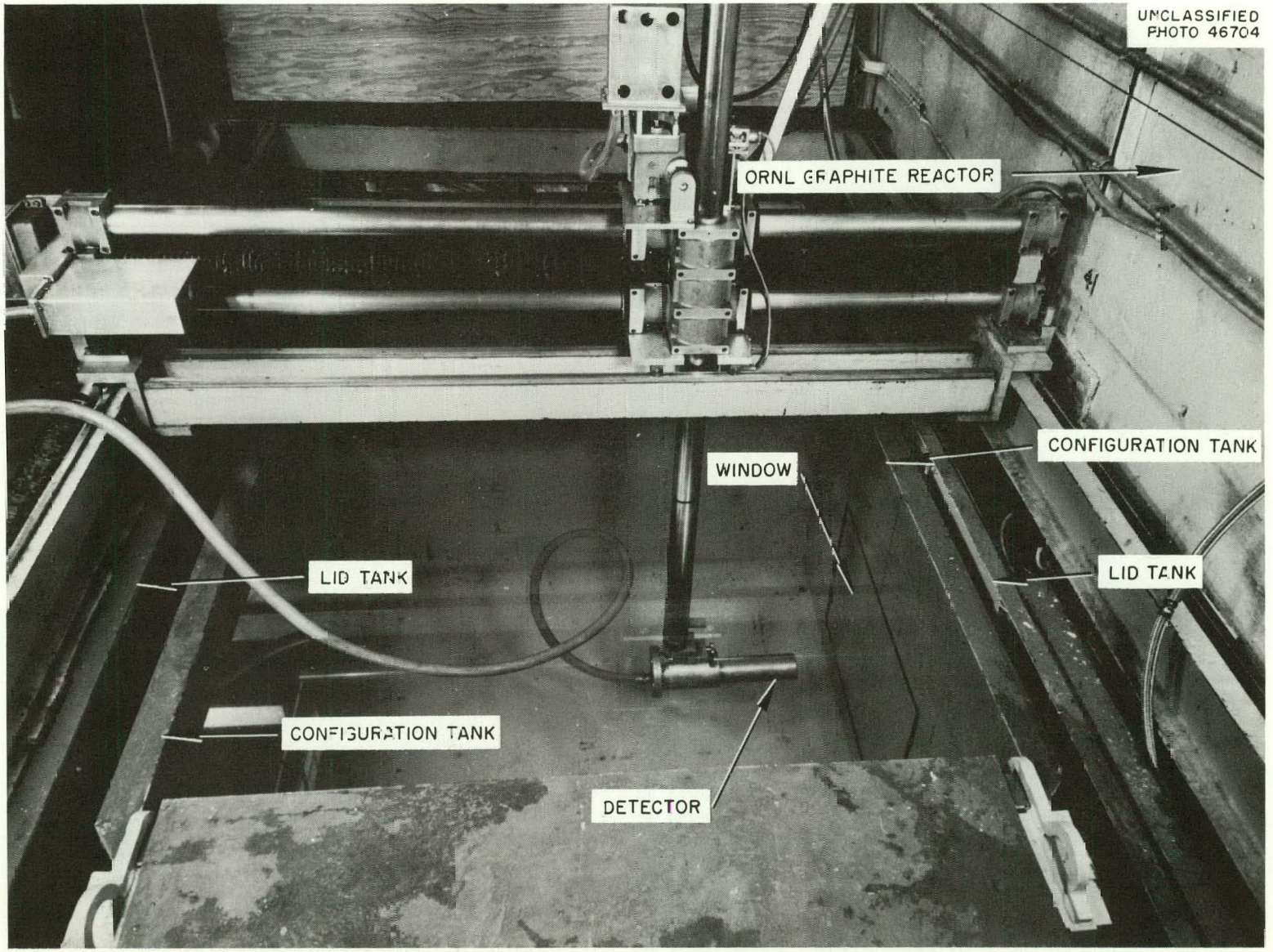

Fig. 1. ORNL Lid Tank Shielding Facility, Showing Configuration Tank in Place.

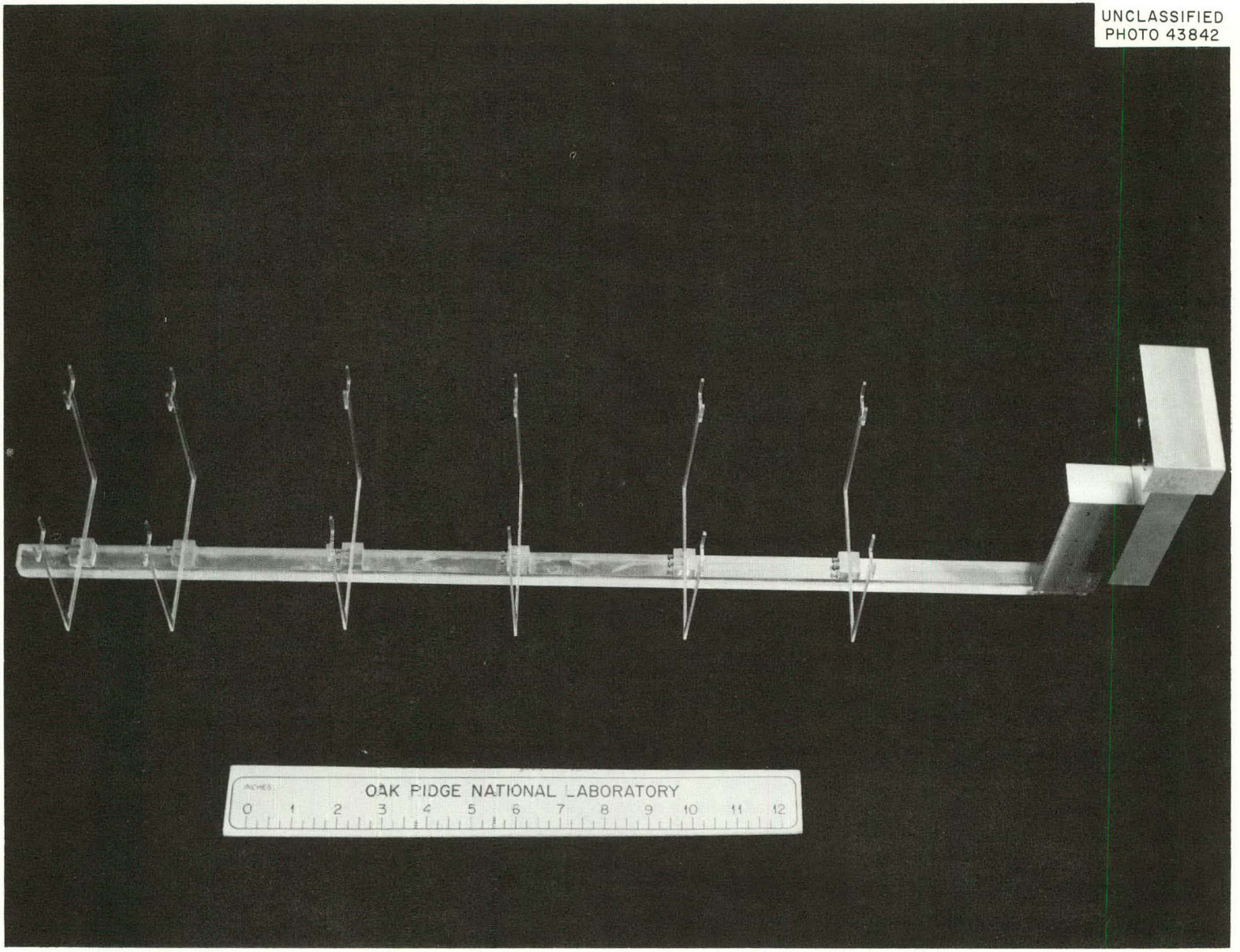

Fig. 2. Foil Holder.

detector shown in Fig. 1. The position of the foil could be determined to ± 0.5 mm in any direction.

For square foil thicknesses < 1.7 mg/cm^2 the foils were prepared by evaporation onto a Mylar film backing, and their masses were determined by colorimetric analysis, with an accuracy of ~5%. The thicker foils were cut from rolled sheets, and their masses determined by weighing, with an accuracy of ± 0.1 mg. The disk-shaped foils were also cut from rolled sheets and their masses determined by weighing to the same accuracy.

The cadmium covers employed for the determination of the epicadmium activity were 0.023 in. thick, which was sufficient to ensure absorption of thermal neutrons. The influence of the cadmium covers on the epicadmium activity was determined in an auxiliary experiment and is discussed later.

Two different gamma-ray counters were used to measure the activation induced in the foils. The square foils and the circular foils with diameters of 0.5 cm and 1 cm were counted with a NaI(Tl) scintillation crystal,[2] 2 in. in diameter, 2 in. in height, and containing a 3/4-in.-diam by 1 1/4-in.-deep well. The effective sensitivity of the counter was changed by inserting a lead sleeve around the sample glass vial into the well for fairly strong sources, or an aluminum spacer sleeve for weaker ones. The counter was calibrated with the aid of a sample of known strength and checked daily to ensure freedom from drift.

---

2. Gratitude is expressed to the Analytical Laboratory, Analytical Chemistry Division, ORNL, for the use of this counter.

The other counter, shown diagrammatically in Fig. 3, was used for those foils having a diameter of 2 or 3 cm. Since the outputs of its two crystals were summed, it was necessary for both to have the same response to the incident gamma rays. The pulse-height output from each photomultiplier was adjusted until the number of pulses from a standard source above an arbitrary bias was the same for both tubes. The bias used for counting the foils was set at a level determined from prior calibration with known gold foils.

The efficiency of the well-type counter had been established by intercalibration with a high-pressure ionization chamber, for which an absolute calibration was available. The efficiency of the two-crystal counter was determined by counting the same foil, first in the ionization chamber and then in the two-crystal counter. This efficiency is a function of the foil diameter as well as the foil thickness.

The foils were exposed at a location in the configuration tank at which the neutron flux was approximately constant with position. Prior to each run a flux traverse was taken along the axis of the source plate by means of a small fission chamber. In one case it was found that the configuration tank had shifted away from the source plate by about 5 mm; data were then taken at a correspondingly corrected distance, so that the total water thickness remained constant. Figure 4 shows the traverses, taken at different times, with the one just mentioned displaced by 5 mm. Since only the shape of the curve is important, the curves were arbitrarily normalized and are therefore slightly separated.

UNCLASSIFIED
ORNL-LR-DWG 52406

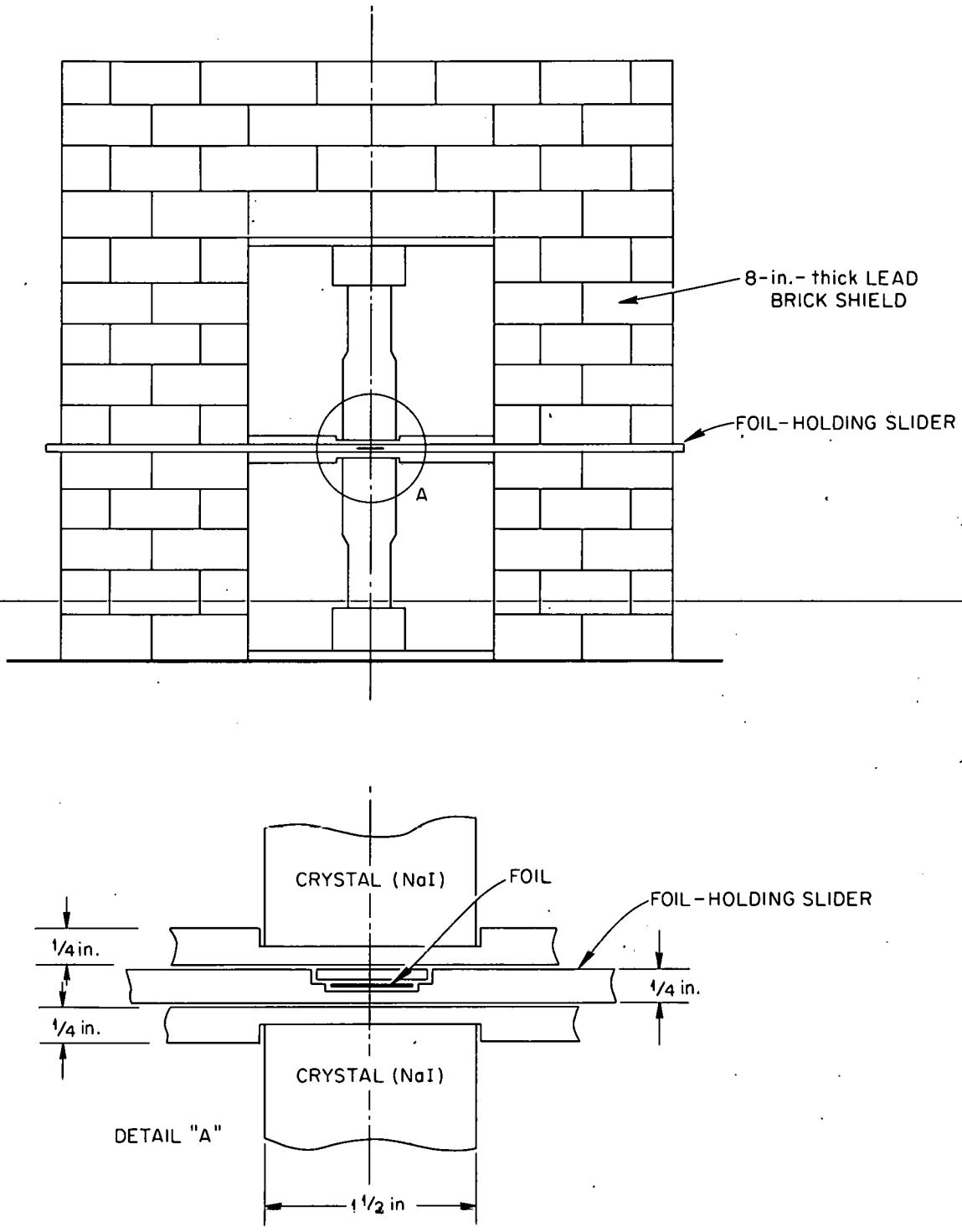

Fig. 3. Two-Crystal Scintillation Counter.

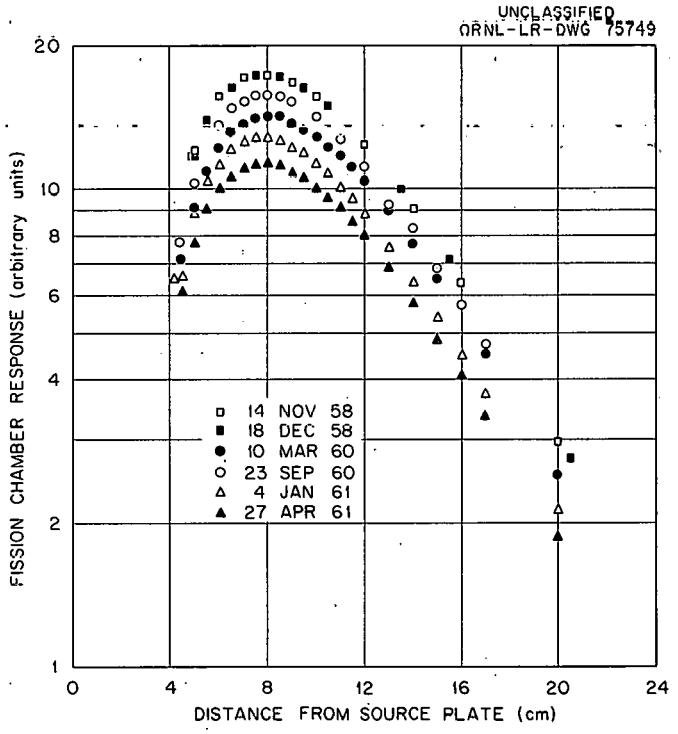

Fig. 4. Neutron Flux Traverses Along Source-Plate Axis.

To check the isotropy of the flux at the chosen position, foils were irradiated at that point, some with flat faces parallel to the source plate and others with flat faces perpendicular to the source. Alternate faces were covered with cadmium. Since the cadmium ratio at that location was about 10, an appreciable anisotropy in the thermal flux should have led to different activities in the foils. Within the limits of experimental error, ~1.5%, no difference could be detected.

The several foil-exposure runs making up this experiment were rather widely separated in time. In order to compare the results, it was necessary to normalize the data from the different runs. There are two normalizations that must be considered: one involving the small short-term fluctuations in the source-plate power during a run, and one which corrects for possible long-term drifts between runs.

The short-term correction is based on the output of a boron-lined ionization chamber which measures the neutron flux incident upon the source plate. While it is known that the output is not quite linear over a large change in reactor power (e.g., from 1700 to 3400 kw), the fluctuations to be expected during a run will not exceed 100 kw, and the linearity of the instrument over that range is adequate.

In the case of the square foils, the long-term normalization was accomplished by using the average of the normalization factors obtained from the ratios of the saturated activities per unit mass of 0.001- and 0.003-in. foils in the different runs. In the case of the circular foils the normalization was based on the comparison of 0.002-in.-thick square

foils exposed during the run for this purpose.

The correction to be applied to the epicadmium activity due to the presence of the cadmium covers was obtained from an auxiliary experiment. Gold foils, 0.002 in. thick and 7/16 in. in diameter, were exposed in cadmium covers 0.019 to 0.070 in. thick. The saturated activity per unit mass was obtained as described above, and the points were fitted to a straight line with a least-squares fitting routine programmed for an IBM-7090. The results are shown in Fig. 5. The intercept at zero cadmium thickness is $(2.107 \pm 0.018) \times 10^8$ dis $min^{-1}g^{-1}$, and the saturated activity per unit mass at 0.023 in., the thickness used in the investigation, is $(2.080 \pm 0.010) \times 10^8$ dis $min^{-1}g^{-1}$. The correction factor is, therefore, 1.013 ± 0.010. This correction was applied to the cadmium-covered activities prior to the fitting of the points.

EXPERIMENTAL RESULTS

The results of the foil activations for the square foils are presented in Figs. 6 and 7, in which the saturated activity per unit foil mass is plotted against foil mass for both the bare and the cadmium-covered foils. Each point shown is the average of four to eight determinations. The data reduction calculations were programmed for the IBM-7090 to reduce the labor involved.

In order to compute the flux depression factor, the value of the unperturbed flux must be known. This value can be obtained from extrapolation to zero foil thickness, for which the flux would not be depressed.

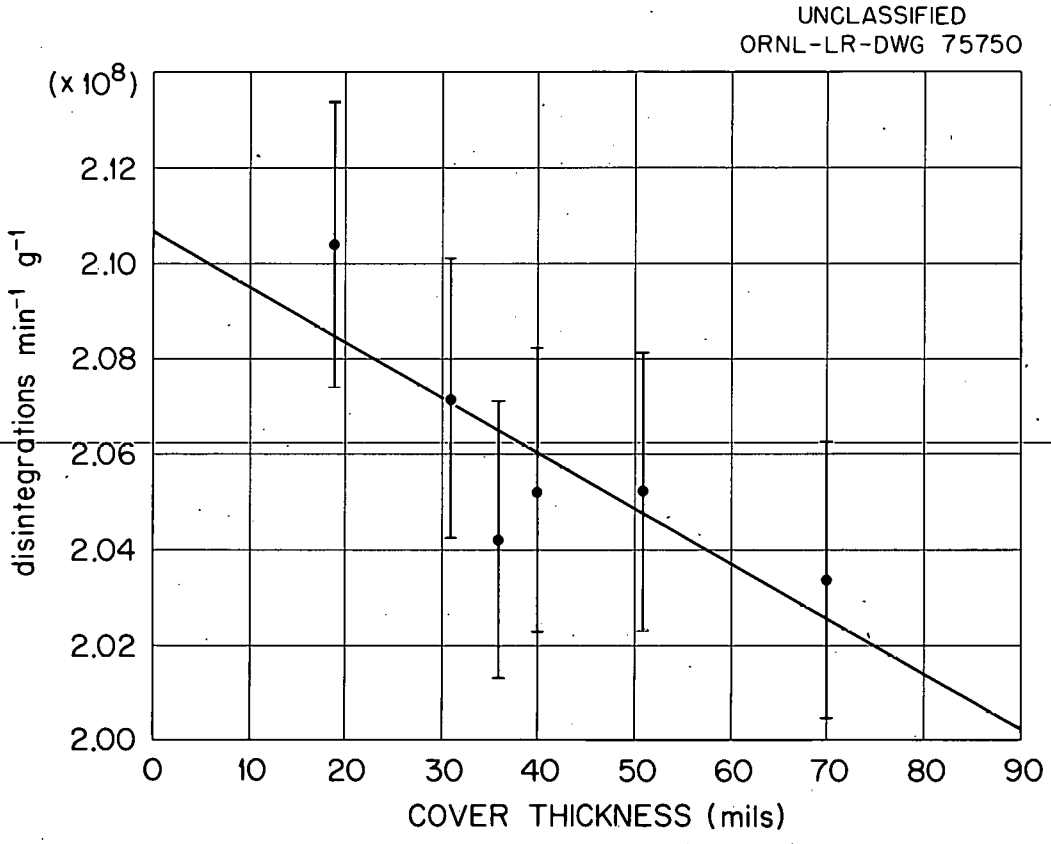

Fig. 5. Foil Activation as a Function of Cadmium Cover Thickness. The straight line is a least-squares fit to the data points.

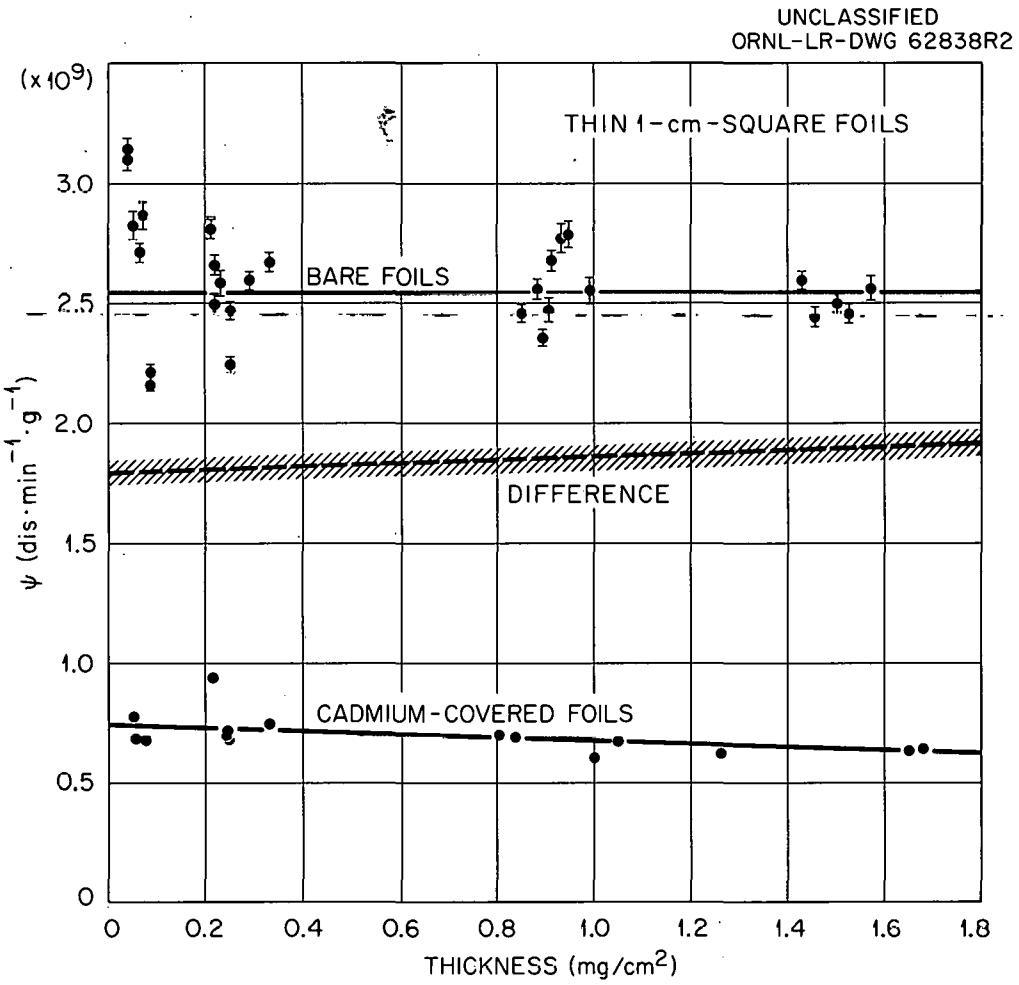

Fig. 6. Saturated Activity per Unit Mass (ψ) as a Function of Foil Thickness for Thin 1-cm-Square Gold Foils in an Isotropic Flux. The solid curves are least-squares fit to the data points; the dashed curve is the difference between the two solid curves; the shaded band indicates the error.

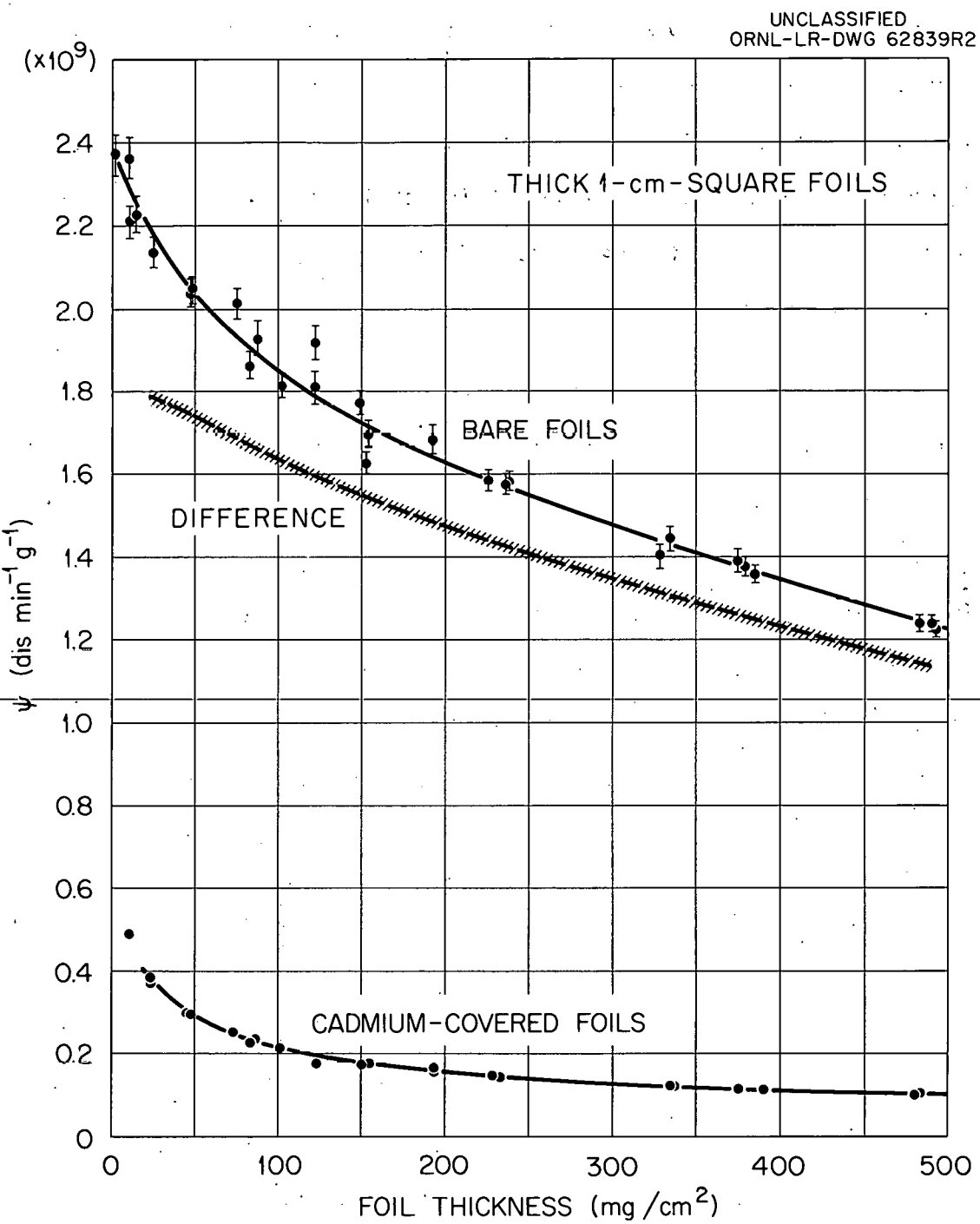

Fig. 7. Saturated Activity per Unit Mass (ψ) as a Function of Foil Thickness for Thick 1-cm-Square Gold Foils in an Isotropic Flux. The solid curves are least-squares fit to the data points; the dashed curve is the difference between the two solid curves; the shaded band indicates the error.

To permit this extrapolation, straight lines were fitted to the thin-foil data by the method of least squares, using the above routine. The thick-foil data were fitted with a sum of exponentials, again using a least-squares program for the IBM-7090.[3] The choice of the function was made on the basis of the simplest smooth function which appeared to fit the experimental data.

To facilitate subtraction of the cadmium-covered activities from the bare ones, the code also computed the value of the function at certain predetermined points, chosen to be the mass of a foil at the thicknesses used. Subtraction of these points should eliminate errors due to small fluctuations in the masses of foils with the same nominal thickness. For the very thin foils, arbitrary masses were chosen at convenient intervals. The errors on these computed points were determined from the errors of the individual points from which the curve was determined and from the scatter of the points about this curve. Details and data are given in Appendix A.

The cadmium difference activation for the thin foils increased with increasing foil mass, which is contrary to all expectations. This anomaly is due to the fact that the least-squares approximation to the bare-foil data resulted in a constant, while that for the cadmium-covered foils decreased as expected. The scatter of the points for foil thicknesses less than 0.3 mg/cm^2 is believed to have been responsible for the peculiar result of the fit to the bare-foil data.

---

3. The author is indebted to R. W. Peelle and R. O. Chester for the use of some of their programs for this work.

With the cadmium-difference activities per unit mass used as computed in this way, the flux depression factor was calculated for each foil thickness used. This factor was taken to be the saturated activity per unit mass for a foil of the finite thickness divided by that for a foil of zero thickness. The least-squares program discussed above was then used to fit the resulting flux depression factors with a function of the form $\left(\sum_{i=0}^{n} a_i x^i\right)^{-1}$. The result of this fitting is shown in Fig. 8. Details and data are given in Appendix A.

The data obtained with circular foils of different diameters were treated in the same way as those for the square foils, except that the value for the unperturbed flux was taken to be the same as that obtained for the square foils and so was not redetermined for each diameter. These data are presented in Figs. 9-16 (see Appendix A for details of the calculation).

To investigate the influence of a flux gradient, some data were taken at a point where the flux decreased with a relaxation length $\lambda = 5.8$ cm. This phase, however, was not extensively pursued. Only square foils, with mass in excess of 1 mg/cm^2, were used, so that the major limitation is the extrapolation to zero-foil thickness. The data were treated in the same manner as described above and are presented in Figs. 17 and 18. Calculational details are given in Appendix A.

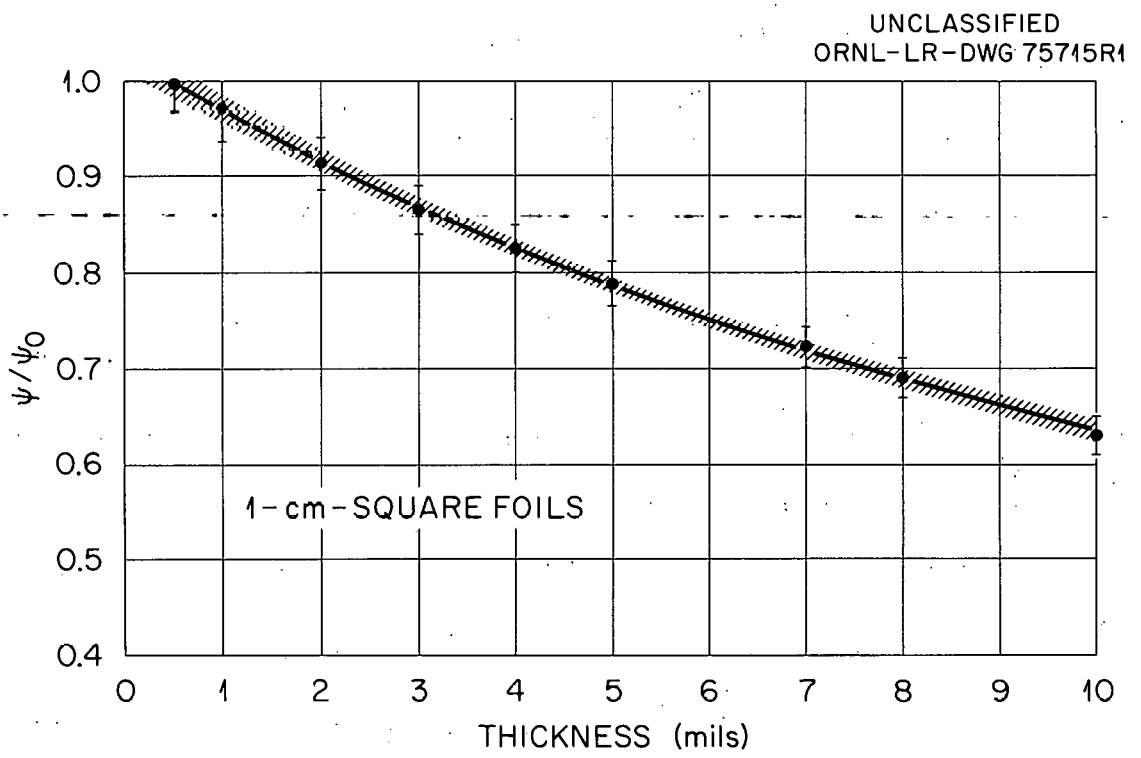

Fig. 8. Experimentally Determined Flux Depression Correction (ψ/ψ_o) for 1-cm-Square Gold Foils in an Isotropic Flux. The curve is a least-squares fit to the points; the shaded band indicates the error.

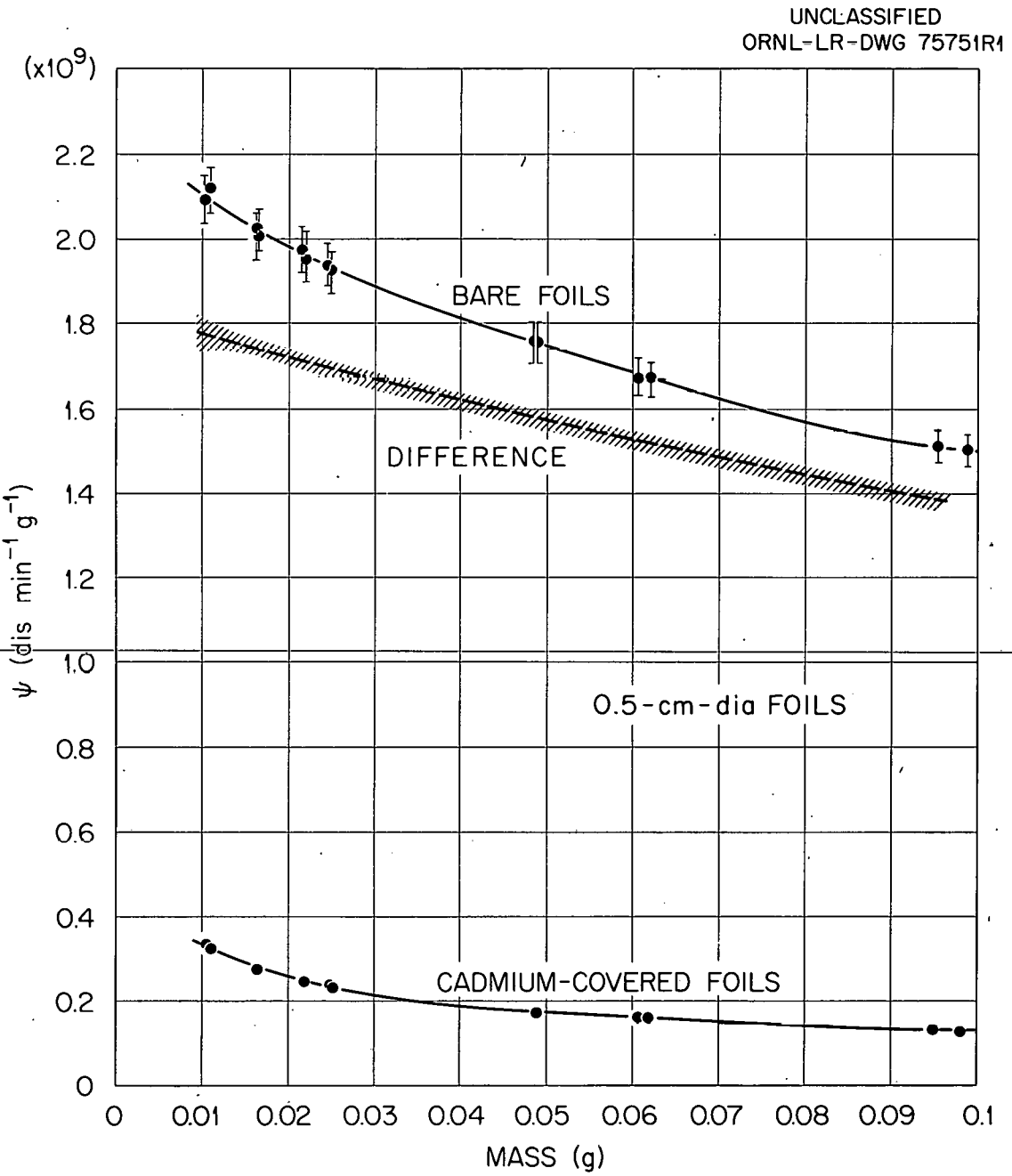

Fig. 9. Saturated Activity per Unit Mass (ψ) as a Function of Foil Thickness for 0.5-cm-diam Gold Foils in an Isotropic Flux. The solid curves are least-squares fit to the data points; the dashed curve is the difference between the two solid curves; the shaded band indicates the error.

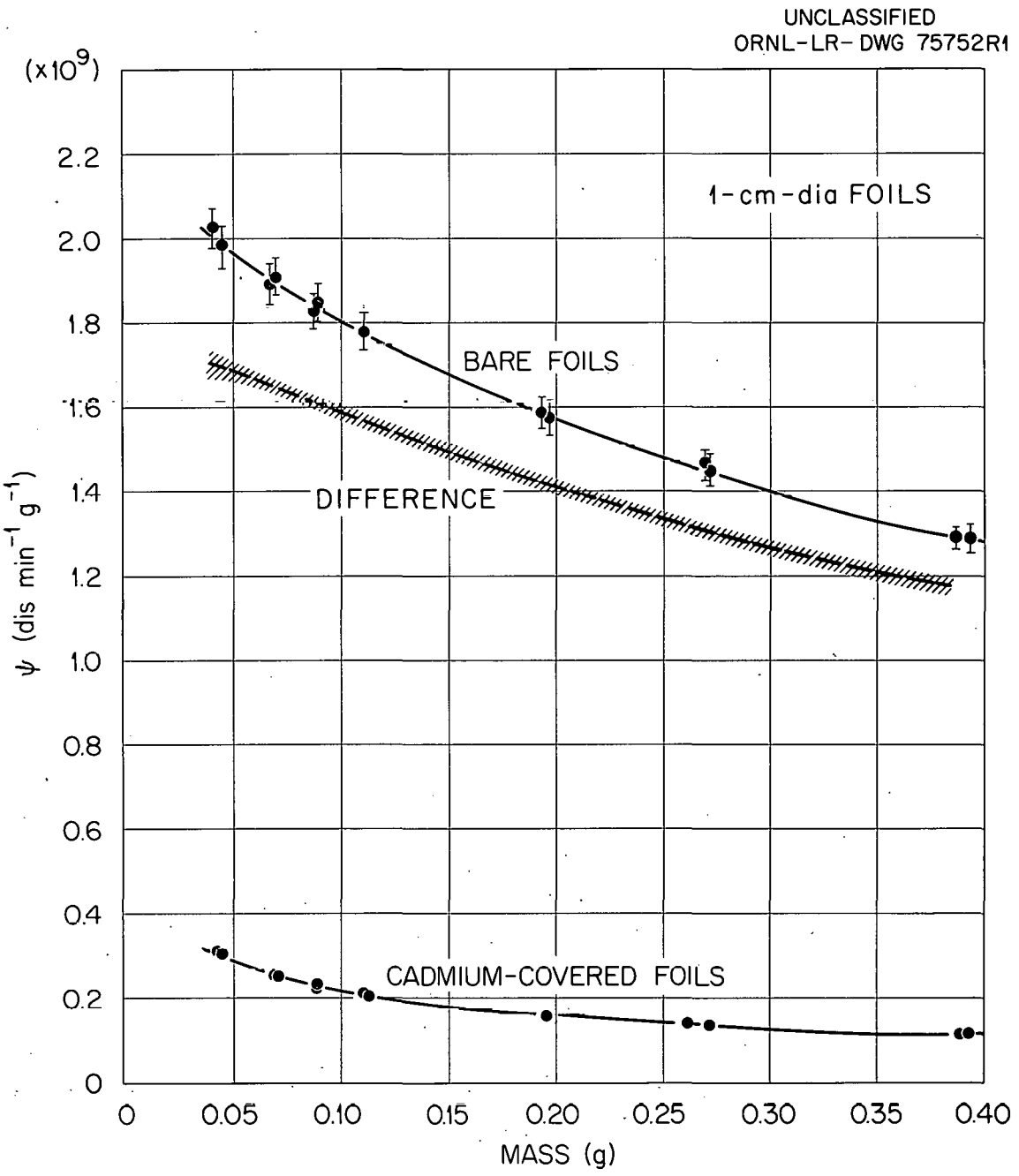

Fig. 10. Saturated Activity per Unit Mass (ψ) as a Function of Foil Thickness for 1-cm-diam Gold Foils in an Isotropic Flux. The solid curves are least-squares fit to the data points; the dashed curve is the difference between the two solid curves; the shaded band indicates the error.

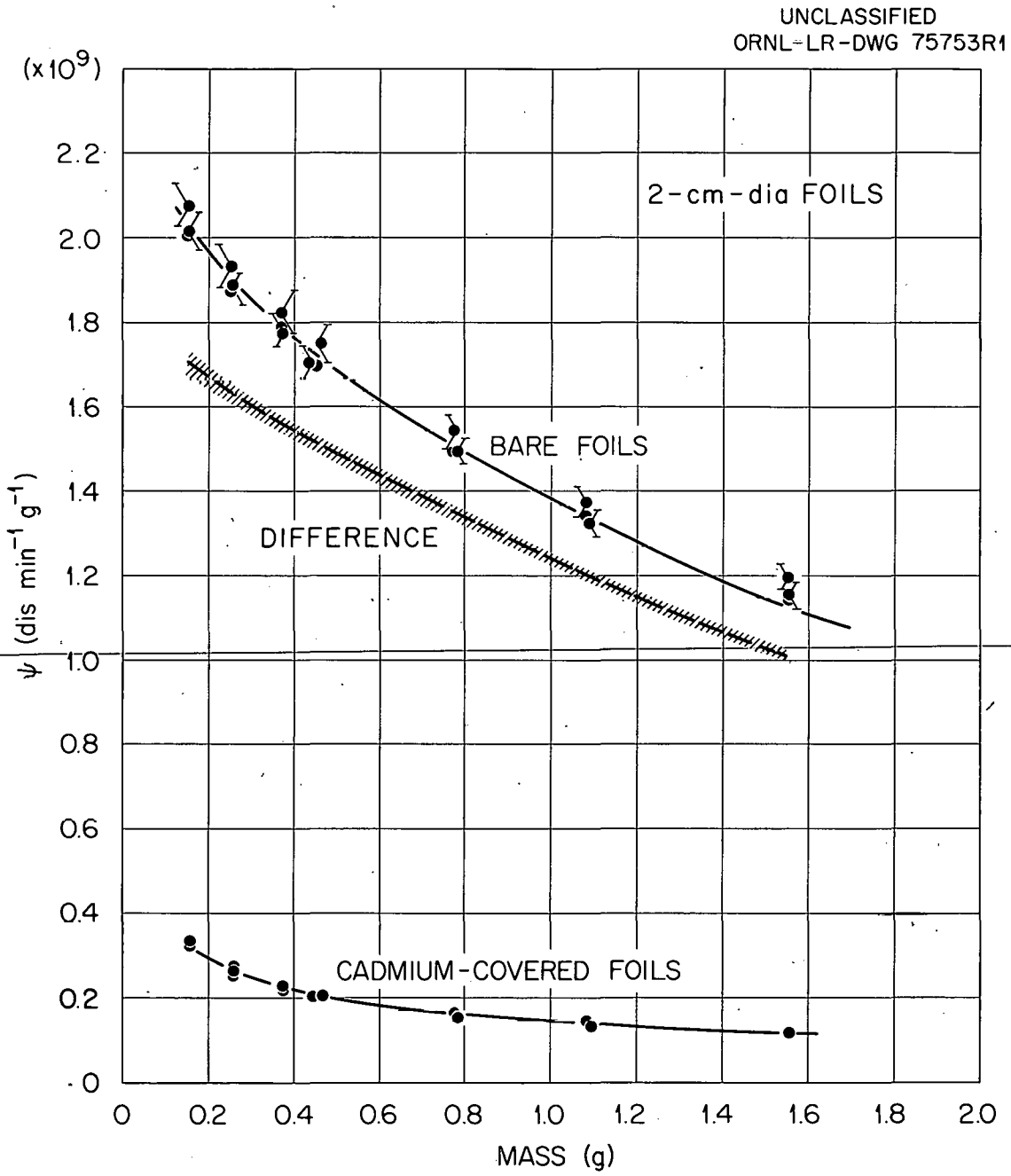

Fig. 11. Saturated Activity per Unit Mass (ψ) as a Function of Foil Thickness for 2-cm-diam Gold Foils in an Isotropic Flux. The solid curves are least-squares fit to the data points; the dashed curve is the difference between the two solid curves; the shaded band indicates the error.

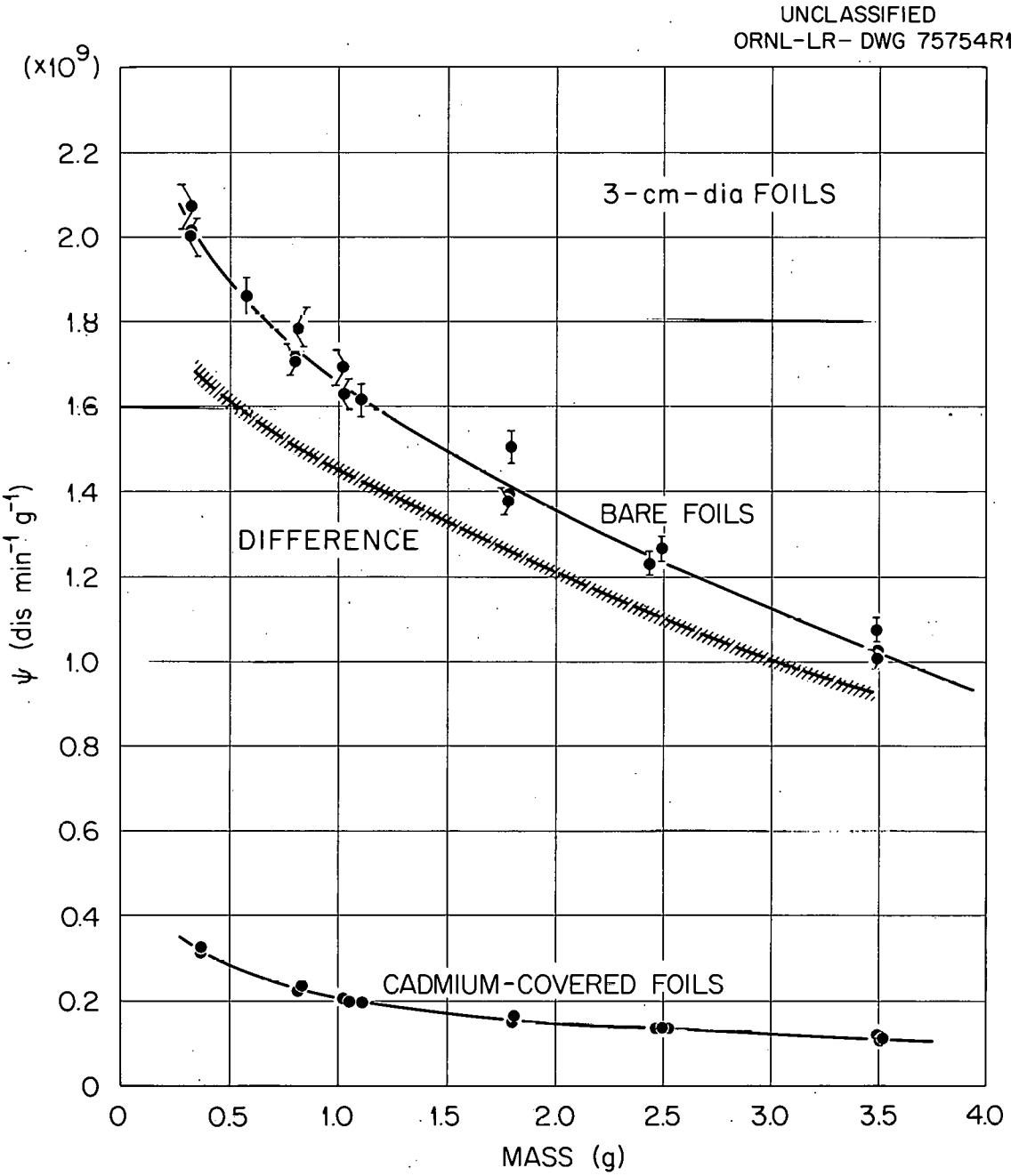

Fig. 12. Saturated Activity per Unit Mass (ψ) as a Function of Foil Thickness for 3-cm-diam Gold Foils in an Isotropic Flux. The solid curves are least-squares fit to the data points; the dashed curve is the difference between the two solid curves; the shaded band indicates the error.

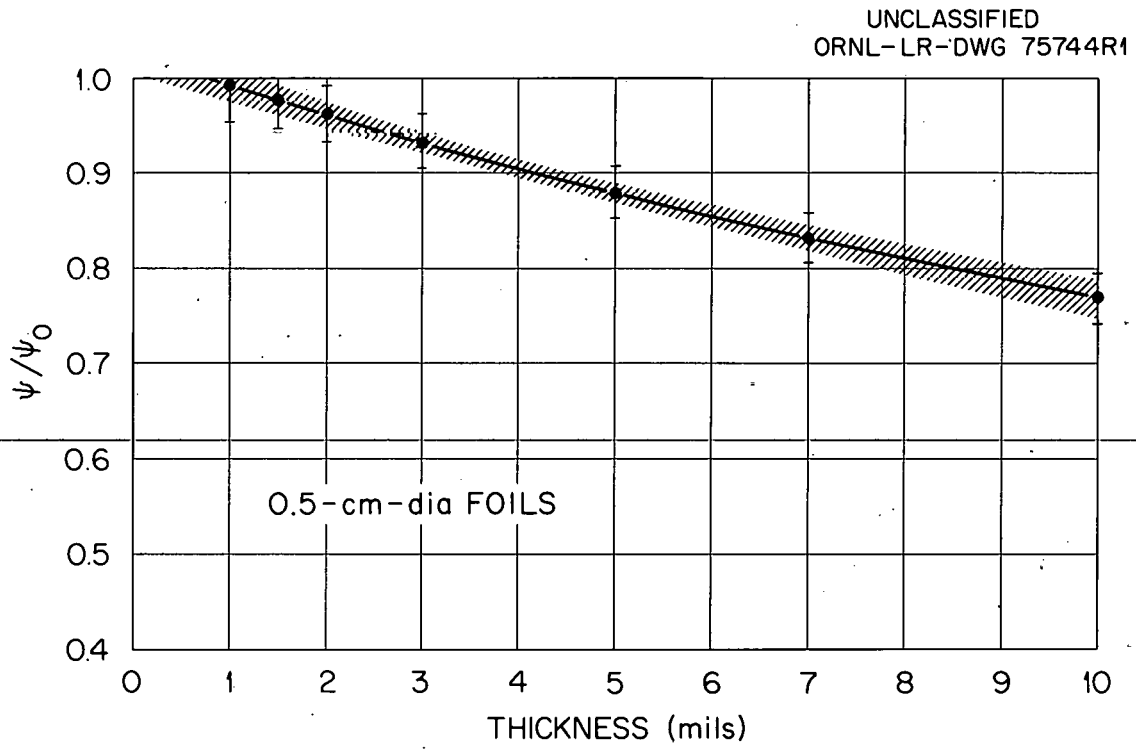

Fig. 13. Experimentally Determined Flux Depression Correction (ψ/ψ_o) for 0.5-cm-diam Gold Foils in an Isotropic Flux. The curve is a least-squares fit to the points; the shaded band indicates the error.

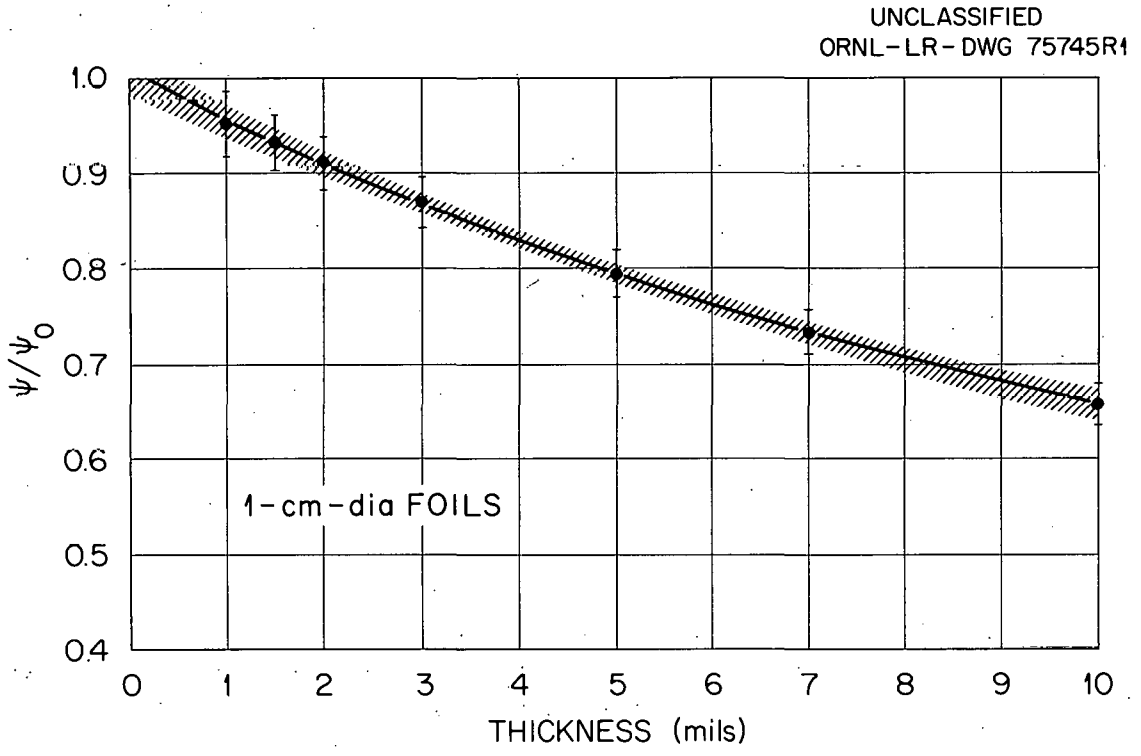

Fig. 14. Experimentally Determined Flux Depression Correction (ψ/ψ_o) for 1-cm-diam Gold Foils in an Isotropic Flux. The curve is a least-squares fit to the points; the shaded band indicates the error.

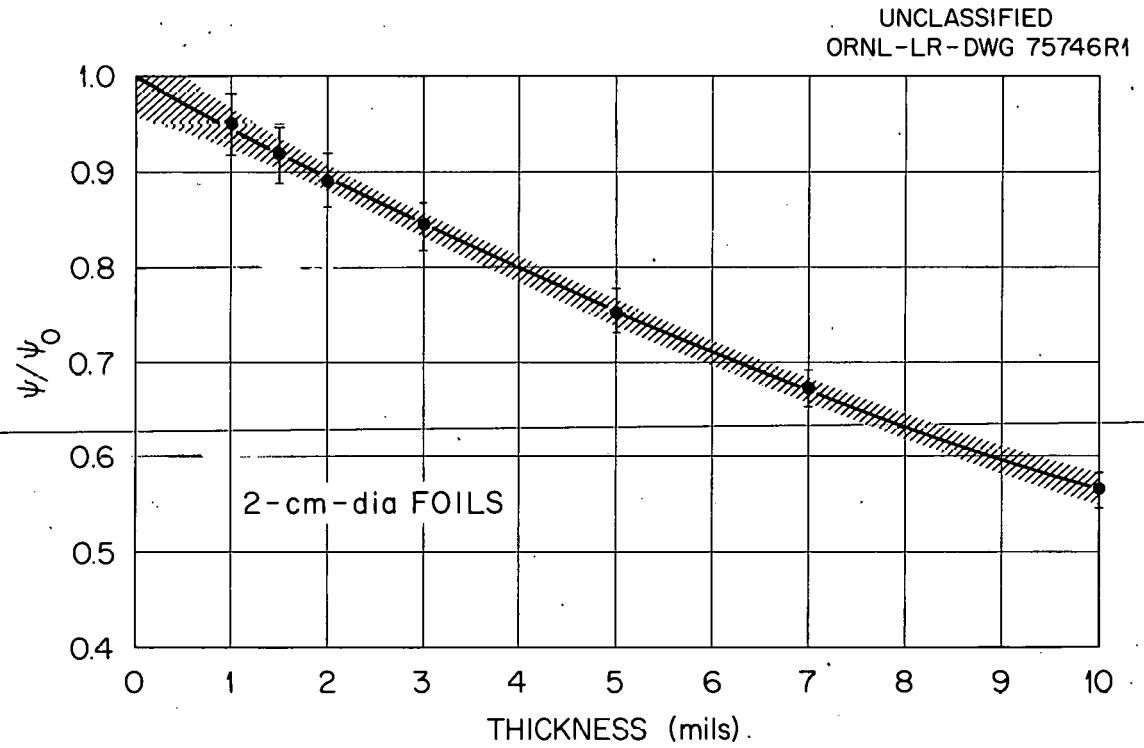

Fig. 15. Experimentally Determined Flux Depression Correction (ψ/ψ_o) for 2-cm-diam Gold Foils in an Isotropic Flux. The curve is a least-squares fit to the points; the shaded band indicates the error.

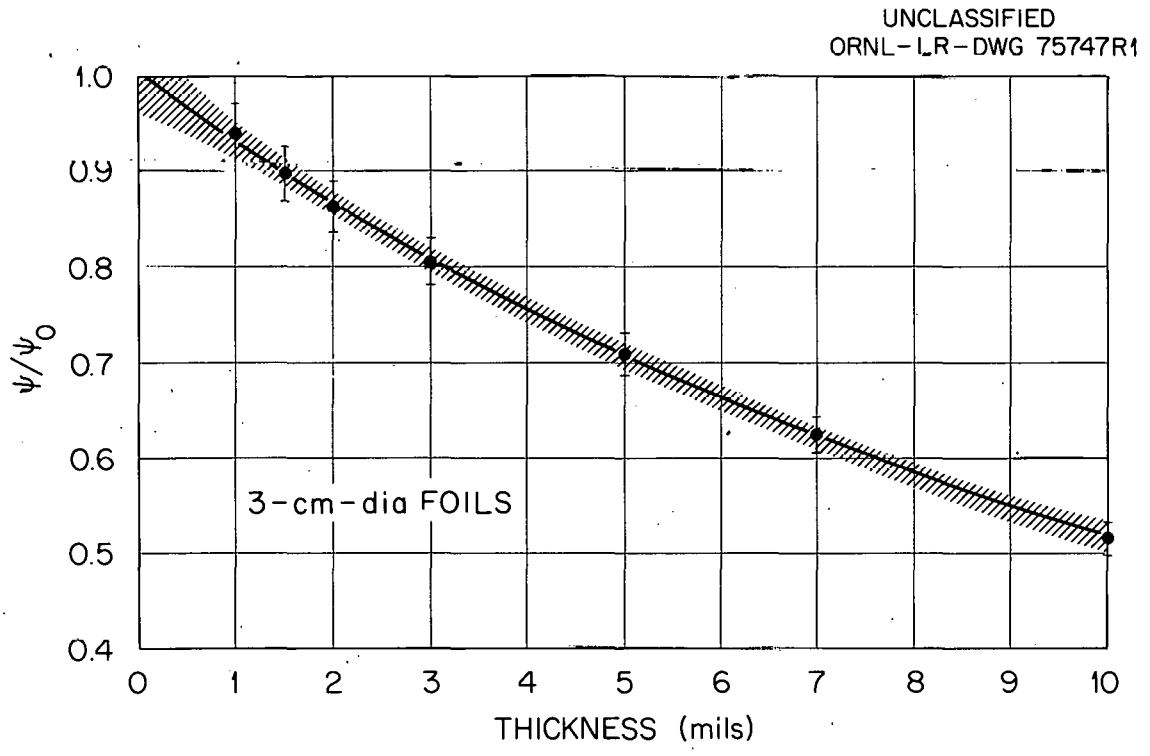

Fig. 16. Experimentally Determined Flux Depression Correction (ψ/ψ_o) for 3-cm-diam Gold Foils in an Isotropic Flux. The curve is a least-squares fit to the points; the shaded band indicates the error.

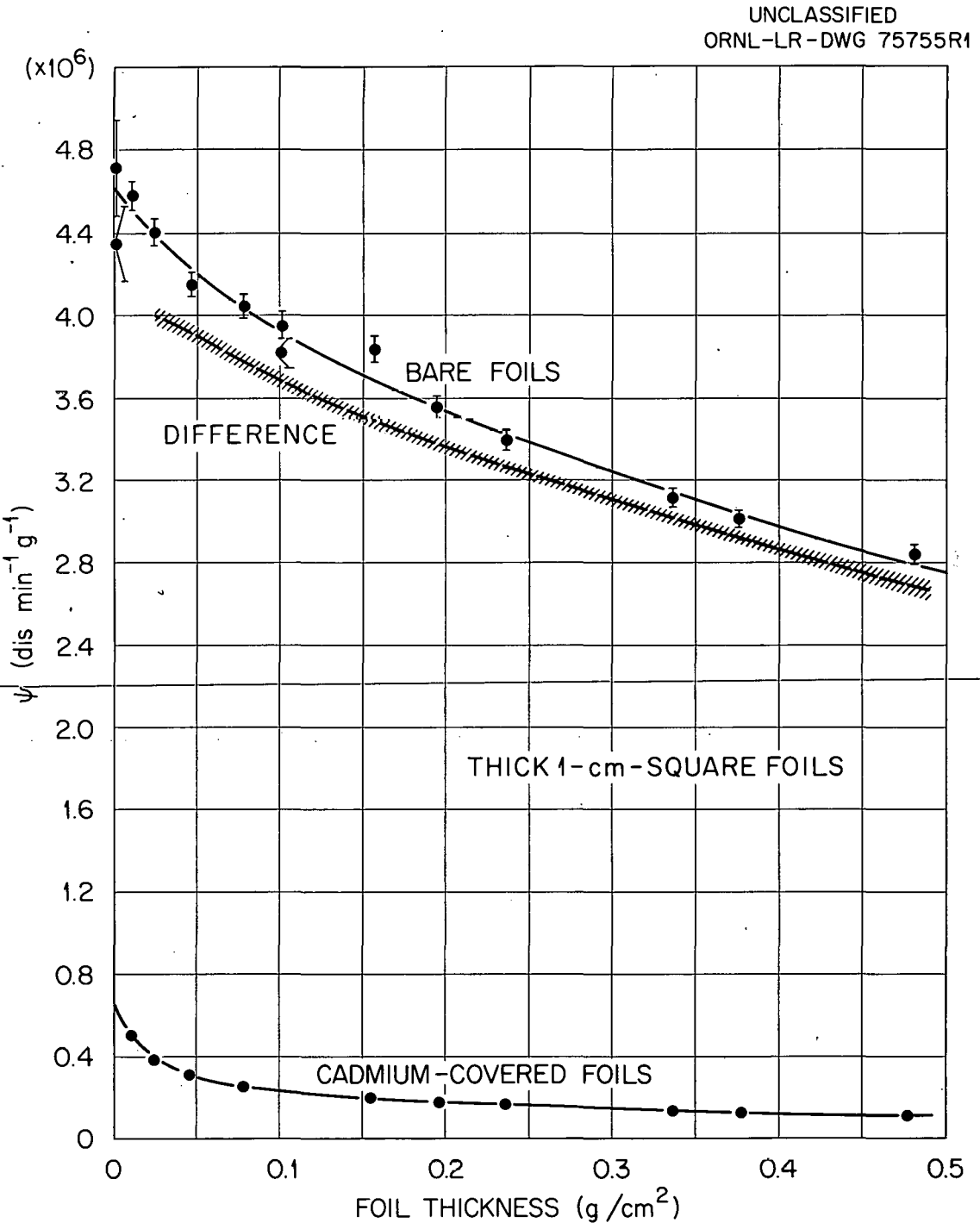

Fig. 17. Saturated Activity per Unit Mass (ψ) as a Function of Foil Thickness for Thick 1-cm-Square Gold Foils in an Anisotropic Flux with Relaxation Length λ = 5.8 cm. The solid curves are least-squares fit to the data points; the dashed curve is the difference between the two solid curves; the shaded band indicates the error.

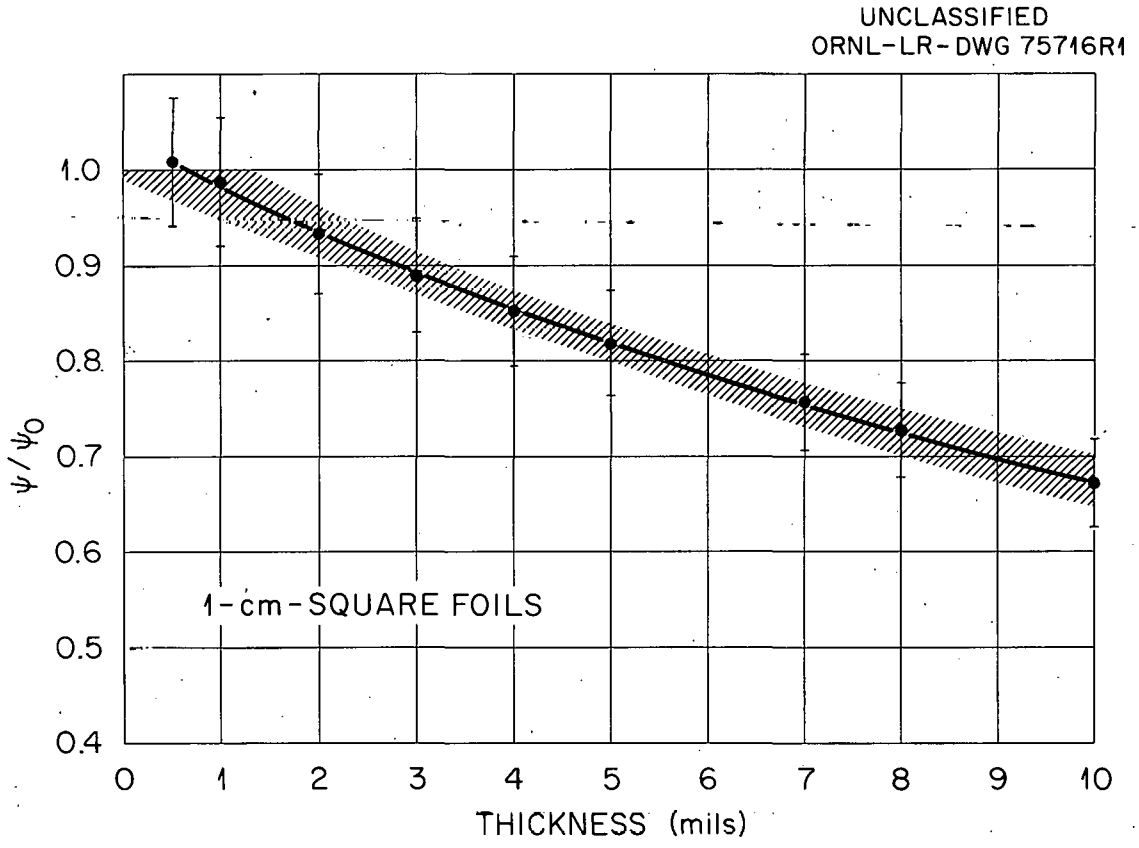

Fig. 18. Experimentally Determined Flux Depression Correction (ψ/ψ_o) for 1-cm-Square Gold Foils in an Anisotropic Flux with Relaxation Length λ = 5.8 cm. The curve is a least-squares fit to the points; the shaded band indicates the error.

COMPARISON WITH THEORY

Probably the earliest attempt to compute the flux depression factor was made by Bothe (9). He considered the case of a spherical detector in an infinite, homogeneous medium. Using diffusion theory calculations, he obtained the flux depression factor

$$f_B = \frac{\alpha_1}{\tau} \left(1 + \frac{3}{2}\alpha_1 \frac{R}{\lambda_s} \frac{L}{R + L} - \alpha_1\right)^{-1}, \qquad (1)$$

where

$$\alpha_1 = \frac{1}{2} - E_3(\tau),$$

$$E_3(\tau) = \int_1^\infty e^{-\tau u} u^{-3} du,$$

$$\tau = \Sigma_a^{Au} x,$$

Σ_a^{Au} = macroscopic absorption cross section of gold,

x = foil thickness,

λ_s = scattering mean free path,

L = diffusion length,

R = radius of spherical detector.

Since practical detectors are disks rather than spheres, he also gave an approximate formula for disks:

$$f_B = \frac{\alpha_1}{\tau}\left[1 + \alpha_1 \left(\frac{a}{\lambda_s} \frac{3L}{2a + 3L} - 1\right)\right]^{-1} \qquad a \gg \lambda_s, \qquad (1a)$$

and

$$f_B = \frac{\alpha_1}{\tau} \left(1 + 0.46\, \alpha_1 \frac{a}{\lambda_s}\right)^{-1} \qquad a \ll \lambda_s \,, \tag{1b}$$

where a is the foil radius and the other terms are defined above.

Bothe's formula was modified somewhat by Tittle (10), who suggested replacing the scattering mean free path λ_s by the transport mean free path λ_{tr}. He also advocated the use of the radius of the disk in Eq. (1) rather than the two-thirds approximation which led Bothe to Eqs. (1a) and (1b). Thus, according to Tittle, Eqs. (1a) and (1b) should be

$$f_T = \frac{\alpha_1}{\tau} \left(1 + \alpha_1 \frac{3a}{2\lambda_{tr}} \frac{L}{a + L} - 1\right)^{-1} \qquad a \gg \lambda_{tr} \,, \tag{2a}$$

and

$$f_T = \frac{\alpha_1}{\tau} \left(1 + 0.68\, \alpha_1 \frac{a}{\lambda_{tr}}\right)^{-1} \qquad a \ll \lambda_{tr} \,. \tag{2b}$$

Skyrme (11) computed the flux depression correction for a finite disk by using the transport theory. In calculating the neutron capture rate in the disk he first neglected the perturbation caused by the foil and then corrected it for thin disks to obtain

$$f_S = \frac{\alpha_1}{\tau} \left[1 - \tau \frac{1}{2} E_1(\tau) + A(g) + D_1 - D_1'\right], \tag{3}$$

where $g = a\Sigma_a^{Au}$; D_1' is small compared with D_1. Graphs are presented in his paper from which $A(g)$ and D_1 may be obtained.

Ritchie and Eldridge (12) calculated the flux depression correction by using a variational method to solve the one-velocity transport equation. Their results may be written

$$f_{RE} = \frac{\alpha_1}{\tau} \left\{ 1 + \alpha_1 g_S \left(\frac{L}{\lambda_T}, a \right) \left[\frac{g_v \left(\frac{L}{\lambda_T}, \tau \right)}{g_S \left(\frac{L}{\lambda_T}, \infty \right)} \right] \right\}^{-1}, \qquad (4)$$

where

$$g_S \left(\frac{L}{\lambda_T}, a \right) = \frac{3L}{2\lambda_T} S \left(\frac{2a}{L} \right) - K \left(\frac{2a}{\lambda_T}, \frac{\Sigma_s}{\Sigma_T} \right),$$

$$\Sigma_s = \frac{1}{\lambda_s},$$

$$\lambda_T = \frac{1}{\Sigma_T},$$

$$\frac{1}{\Sigma_T} = \text{total mean free path},$$

and S, K, and g_v/g_S^{∞} are obtained from graphs given in their paper.

The latest theoretical approach to the flux depression problem was made by Dalton and Osborn (13). They converted the one-velocity transport equation to an iterative integral equation, which could then be solved with the aid of a digital computer.

Before the experimental data can be compared with the theoretical predictions, an additional correction must be applied to take account of the gamma-ray self-absorption effect. To determine this factor, foils of the same thickness as the (nominal) 0.005-, 0.007-, and 0.010-in. foils were made up from stacks of (nominal) 0.001- and 0.0015-in. foils, 2 and 3 cm in diameter. These stacks were counted in the container and then taken apart and the individual foils counted separately. For each nominal thickness the self-absorption was calculated from the ratio of the sum of the counts of the individual foils to the counts of the stack, after appropriate corrections had been made for the decay time. Agreement between the data for the 2- and 3-cm-diam foils was excellent. The averages of these data as a function of thickness were fitted to a straight line, and the corrections so determined were applied to all foils as indicated. The correction as a function of thickness is shown in Fig. 19.

It is tempting to use a very simple calculation to obtain these corrections. One assumes that the source is concentrated in the midplane of the foil and that the gamma rays are emitted normally. The corrections so obtained are substantial underestimates of the measured self-absorption factors.

Hanna (14) recently pointed out the importance of the "flux hardening" effect in the foil. This effect must be considered in the proper averaging of the cross sections over the energy distribution of the neutrons; however, for the calculations shown in this report, the following values were used:

$$\Sigma_a^{Au} = 5.17 \text{ cm}^{-1} , \quad \text{from Dalton and Osborn (13)}$$

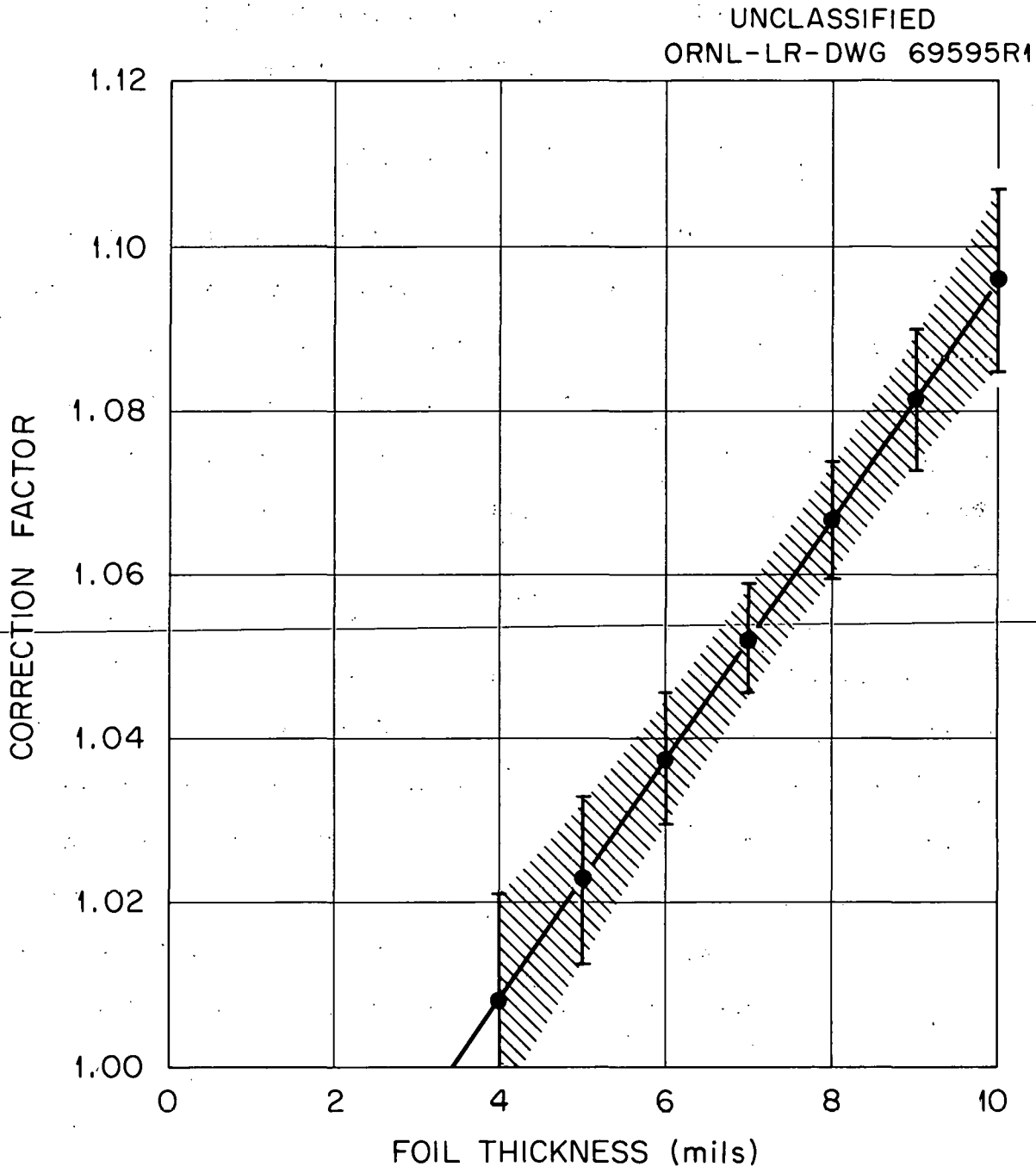

Fig. 19. Correction Factor for the Absorption of the 411-kev Gamma Radiation in the Gold Foil as a Function of Foil Thickness. The line is a least-squares fit to the points; the shaded band indicates the error.

$\lambda_s = 0.320$ cm , from Dalton and Osborn (13)

$L = 2.714$ cm , from H. H. Baucom, Jr. (15)

$\lambda_T = 0.318$ cm , from Dalton and Osborn (13)

$\lambda_{tr} = \frac{3D_o}{v} = 0.483$, from Küchle (16)

The choice of these particular values is governed by the ones used by Dalton and Osborn (13), whose results are not given in a form to be easily susceptible to a change in the input parameters. The effect of flux hardening was not considered by them in the computation of the average cross sections and therefore is not considered in this paper. The remaining constants were chosen so as to provide a consistent set.

The curves, calculated according to the above theories, and the experimental data corrected for the self-absorption are shown in Figs. 20-24. For calculation purposes the square foils were converted to circular ones of equal area, except for the Dalton-Osborn method of calculation. In most cases two curves are given for the Dalton-Osborn approach. In one case, isotropic scattering in the water was assumed, as it was for all the other theories. In the other case, Dalton (17) recalculated his curves to include the anisotropy of the scattering, using $\bar{\mu} = 0.3$.

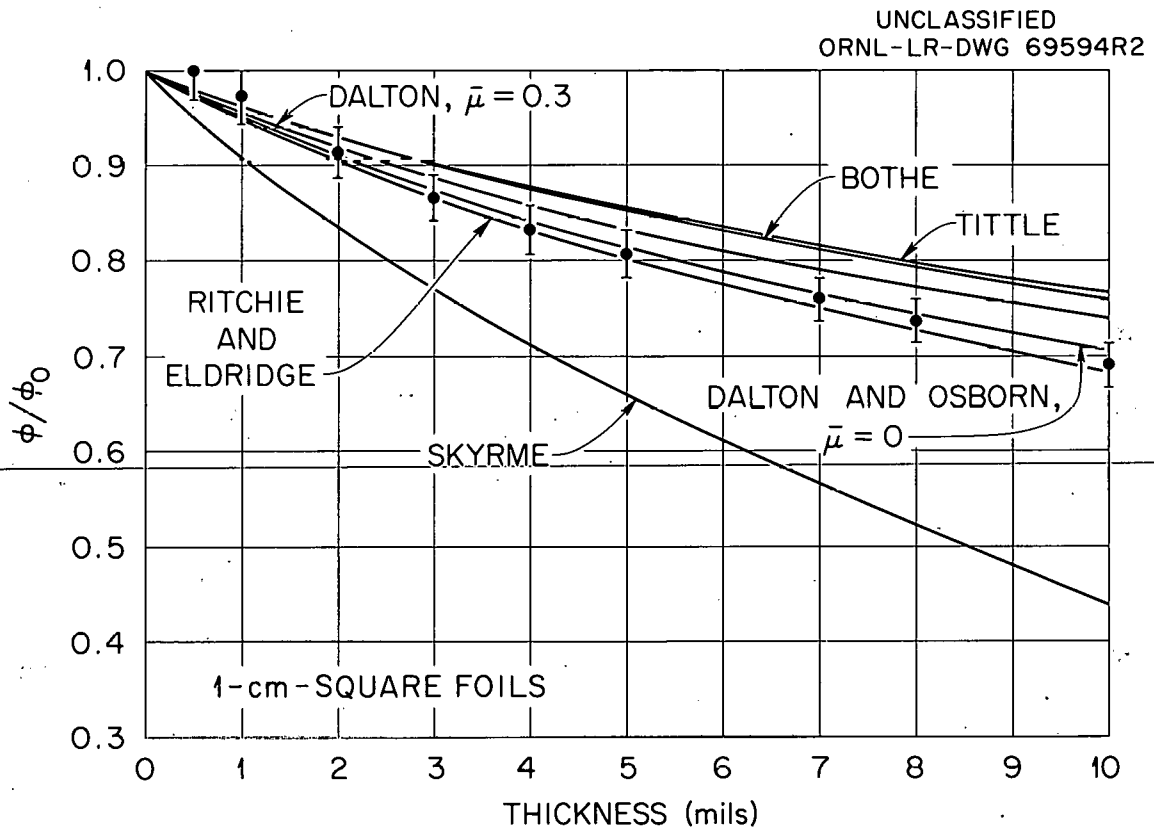

Fig. 20. Experimentally Determined Flux Depression Factors (Corrected for Self-Absorption) for 1-cm-Square Gold Foils in an Isotropic Flux Compared with Theories.

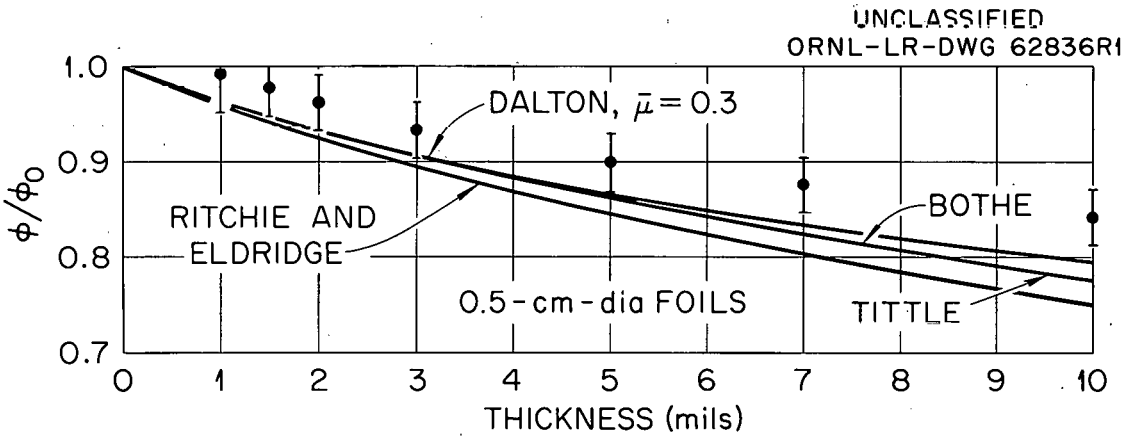

Fig. 21. Experimentally Determined Flux Depression Factors (Corrected for Self-Absorption) for 0.5-cm-diam Gold Foils in an Isotropic Flux Compared with Theories. (Note that the Bothe and Tittle theories yield the same results.)

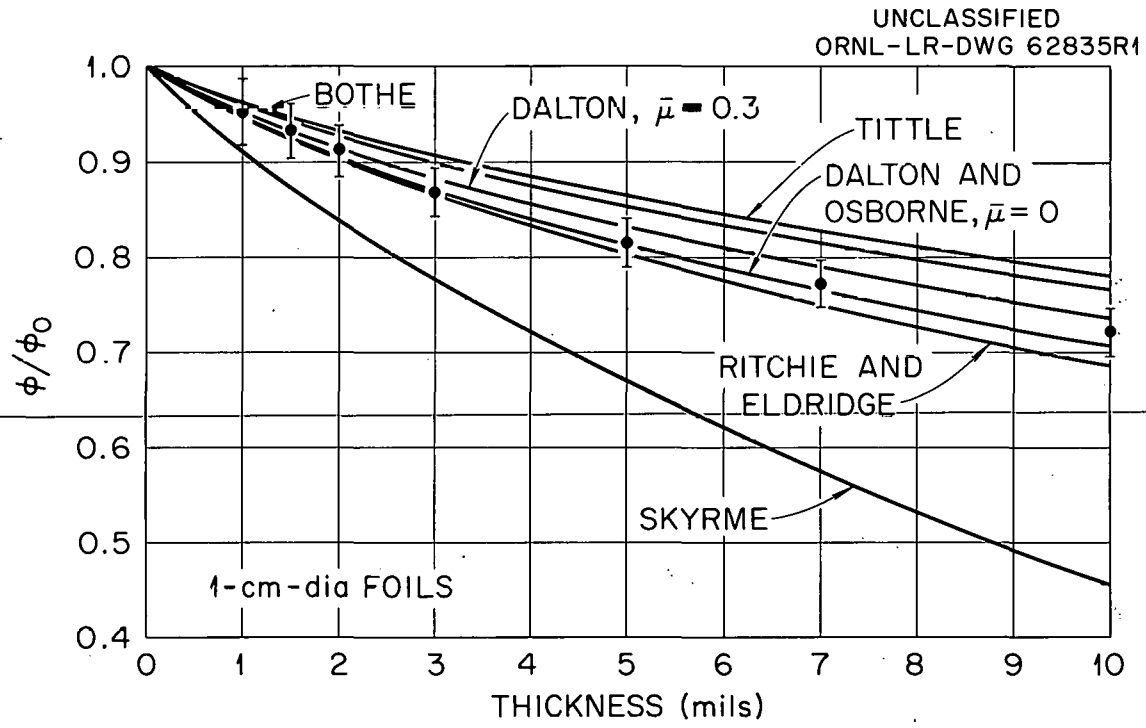

Fig. 22. Experimentally Determined Flux Depression Factors (Corrected for Self-Absorption) for 1-cm-diam Gold Foils in an Isotropic Flux Compared with Theories.

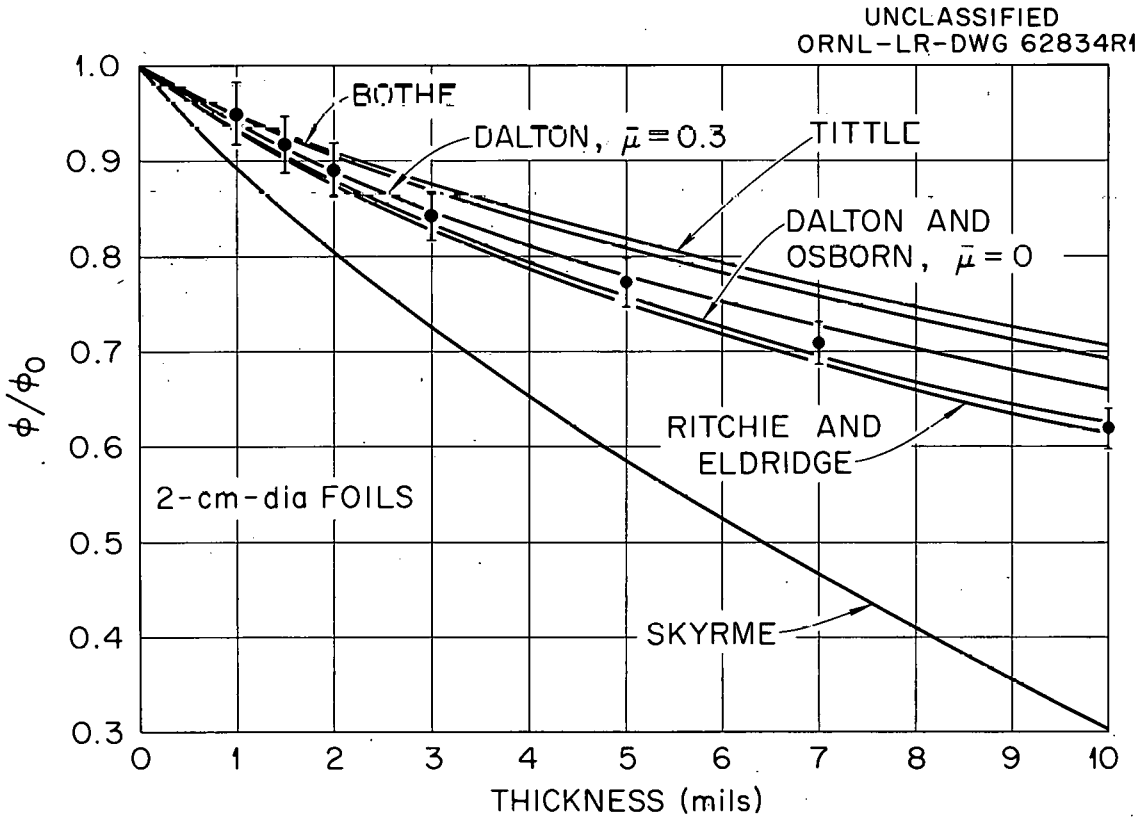

Fig. 23. Experimentally Determined Flux Depression Factors (Corrected for Self-Absorption) for 2-cm-diam Gold Foils in an Isotropic Flux Compared with Theories.

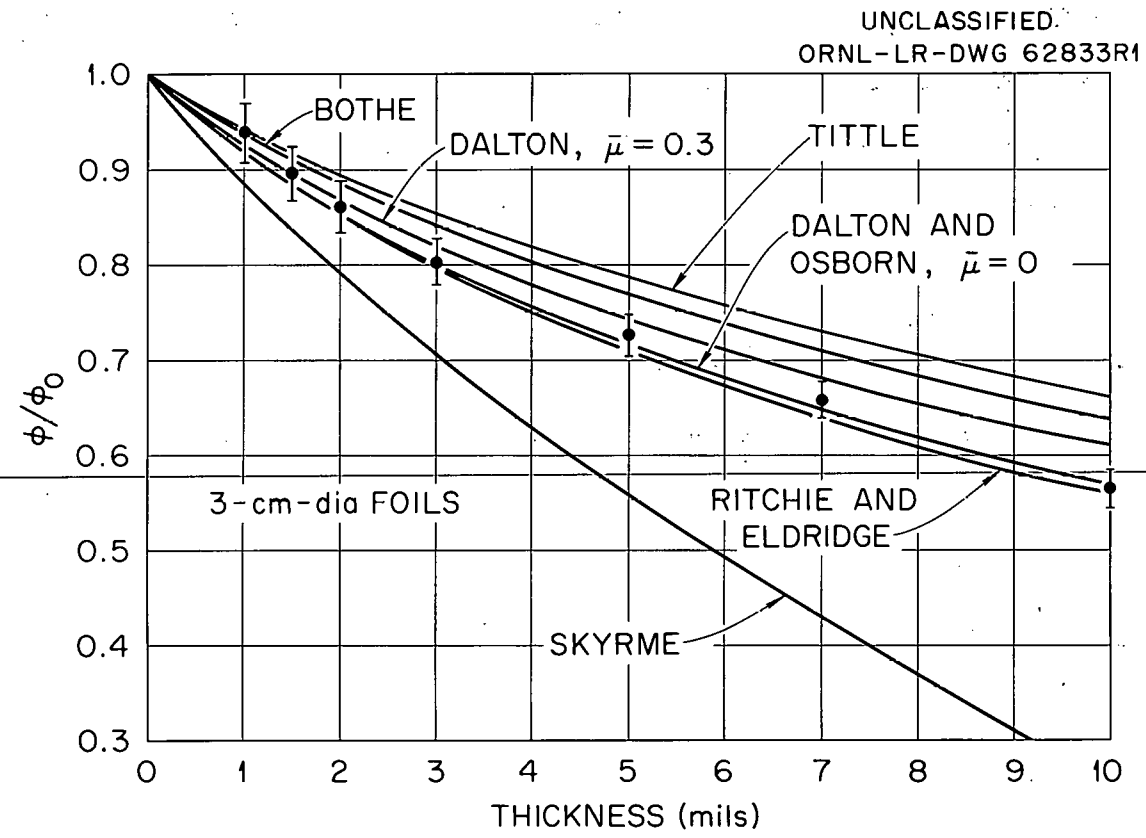

Fig. 24. Experimentally Determined Flux Depression Factors (Corrected for Self-Absorption) for 3-cm-diam Gold Foils in an Isotropic Flux Compared with Theories.

CONCLUSIONS

A comparison of the experimental data for the flux perturbation caused by gold foils in a water medium with theoretical predictions indicates that good agreement can be found with the calculations of Ritchie and Eldridge (12). In view of the underlying assumptions of the theory (one-speed isotropic scattering in the water, no scattering in the foil, approximate correction for finite foil radius), the good agreement must be considered at least partially fortuitous.

The agreement of the experiment with the calculations of Dalton and Osborn (13) is about as good as with those of Ritchie and Eldridge. The Dalton-Osborn results also are computed for the case of isotropic scattering in water; so again the agreement appears fortuitous. This is emphasized by the additional calculations of Dalton (17) for anisotropic scattering, which give poorer agreement in those cases where both calculations have been made.

The other theories outlined above (9-11) give results which diverge from the experimental results, especially for thick (> 0.003-in.) foils.

No theory is available with which to compare the data taken in a nonisotropic flux. The experimental data are compared with those in an isotropic flux in Fig. 25. While the data are consistent within the limits of error, it appears that the slope of the curve in the isotropic case is steeper than in the nonisotropic case. More detailed measurements are required, however, before this point can be confirmed.

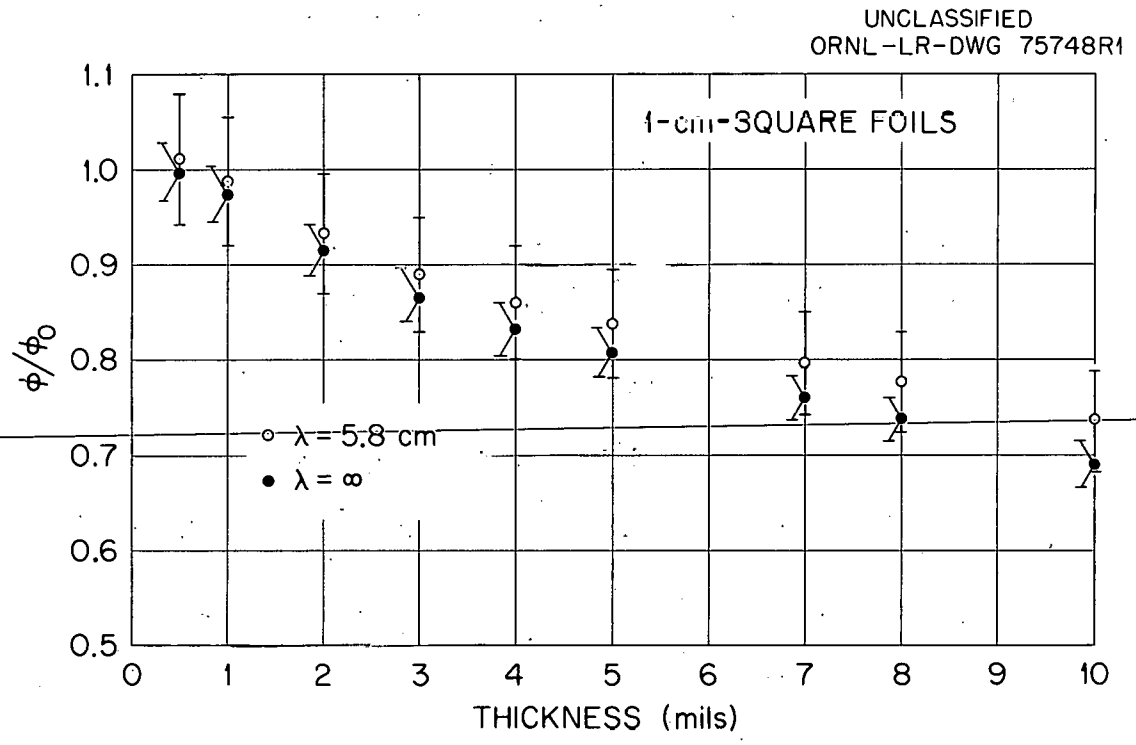

Fig. 25. Comparison of Experimentally Determined Flux Depression Factors (Corrected for Self-Absorption) for 1-cm-Square Gold Foils in an Isotropic Flux ($\lambda = \infty$) and an Anisotropic Flux ($\lambda = 5.8$ cm).

REFERENCES

1. E. D. Klema and R. H Ritchie, Phys. Rev. 87, 167 (1952).

2. A. de Troyer and G. C. Tavernier, Acad. Roy. Sci. Belgique Bull. 39, 880 (1953).

3. H. Meister, Z. Naturforschg. 10a, 669 (1955).

4. M. W. Thompson, J. Nuclear Energy 2, 286 (1956).

5. M. A. Greenfield, R. L. Koontz, and A. A. Jarrett, Nuclear Sci. and Eng. 2, 246 (1957).

6. T. L. Gallagher, Nuclear Sci. and Eng. 3, 110 (1958).

7. A. Sola, Nucleonics 18(3), 78 (1960).

8. H. Goldstein, Fundamental Aspects of Reactor Shielding, p.93, Addison-Wesley, New York, 1959.

9. W. Bothe, Z. Physik 120, 437 (1943).

10. C. W. Tittle, Nucleonics 8(6), 5 (1951); Nucleonics 9(1), 60 (1951).

11. T. H. R. Skyrme, Reduction in Neutron Density Caused by an Absorbing Disc, MS-91 (n.d.).

12. R. H. Ritchie and H. B. Eldridge, Nuclear Sci. and Eng. 8, 300 (1960).

13. G. R. Dalton and R. K. Osborn, Nuclear Sci. and Eng. 9, 198 (1961).

14. G. C. Hanna, Nuclear Sci. and Eng. 11, 338 (1961).

15. H. H. Baucom, Jr., Nucleonics 18(11), 198 (1960).

16. M. Küchle, Nukleonik 2, 131 (1960).

17. G. R. Dalton, University of Florida, private communication.

APPENDIX A

The saturated activity per unit mass was computed from the relation

$$\psi \equiv \frac{A_s}{m} = \frac{\left(\frac{N_c}{t_c} - \frac{N_B}{t_B}\right)\epsilon F}{mMe^{-\lambda t_D}(1 - e^{-\lambda t_b})}, \qquad (A.1)$$

where

N_c = number of counts of foil and background,

t_c = foil counting time (min),

N_B = number of counts of background,

t_B = background counting time (min),

ϵ = counter efficiency,

F = counter normalizing factor,

m = foil mass (g),

M = monitor reading,

λ = decay constant for Au^{198} [= $(1.782 \pm 0.002) \times 10^{-4}$ min^{-1}],

t_D = decay time (min),

t_b = bombarding time (min).

The variance of the saturated activity was computed from the relation

$$V(\psi) = \psi^2 \left\{ \frac{\left(\frac{N_c}{t_c} - \frac{N_B}{t_B}\right)^2 F^2 V(\epsilon) + \left(\frac{N_c}{t_c} - \frac{N_B}{t_B}\right)^2 \epsilon^2 V(F) + \epsilon^2 F^2 \left(\frac{N_c}{t_{c^2}} + \frac{N_B}{t_{B^2}}\right)}{\left(\frac{N_c}{t_c} - \frac{N_B}{t_B}\right)^2 \epsilon^2 F^2} \right.$$

$$+ \left(\left[e^{-\lambda t_D} (1 - e^{-\lambda t_b}) M \right]^2 V(m) + \left[(1 - e^{-\lambda t_b})\, m e^{-\lambda t_D} \right]^2 V(M) \right. \tag{A.2}$$

$$\left. \left. + \left[mM(1 - e^{-\lambda t_b}) \right]^2 x \left[t_D\, \sigma(\lambda)\, e^{-\lambda t_D} \right]^2 + (mMe^{-\lambda t_D})^2 \left[t_b\, \sigma(\lambda) e^{-\lambda t_b} \right]^2 \right) \right.$$

$$\left. x \frac{1}{\left[mMe^{-\lambda t_D} (1 - e^{-\lambda t_b}) \right]^2} \right\} .$$

The errors associated with the various quantities are as follows:

Quantity	Error
ϵ	3%
F	1%
N_c	$\sqrt{N_c}$
N_B	$\sqrt{N_B}$
m	5% for m < 1.7 mg 10^{-4} g for m > 1.7 mg
M	2×10^{-3}
λ	2×10^{-7} min^{-1}

Since F was defined for the well counter only, it was set equal to 1 for foils counted on the two-crystal counter. The error associated with the two-crystal points therefore should be a slight overestimate, since the error calculation was not changed.

The results of these calculations were then normalized and corrected for the cadmium covers, as required. Tables A.1 through A.4 list the final results, which were used as the input data to the curve-fitting programs.

The thin square foil data (Table A.1) were used to fit the expression

$$\psi = a_o + a_1 m \qquad (A.3)$$

by using a weighted least-squares fit. The weight for each point was taken to be $1/[\sigma(\psi)]^2$. The routine also gave an interpolated value of the saturated activity per unit mass, ψ_c, for given values of m according to relation (A.3), as well as the error associated with each such computed ψ_c from the relation

$$\sigma(\psi_c) = \left\{ (\text{SSRM}) \left[((m))^T ((V)) ((m)) \right] \right\}^{1/2}, \qquad (A.4)$$

where

SSRM = (weighted sum of squared residuals)/(degrees of freedom),

$((m))$ = matrix of $\partial\psi/\partial a_i$,

$((V))$ = coefficients' covariance matrix.

The coefficients, SSRM, and $((V))$ are given in Table A.5.

The data obtained with thick square foils, as well as those from circular foils of different diameters, were used to fit

$$\psi = a_o + \sum_{i=1}^{n} a_{2i-1} e^{-a_{2i} m} \quad . \qquad (A.5)$$

Again, ψ_c was computed for given values of m from Eq. (A.5) and the associated error from Eq. (A.4). The results of this fitting procedure, in a form similar to that above, are given in Tables A.6 - A.11.

The flux depression corrections were calculated from the ψ_c values and are given in Table A.12. These correction factors have not been modified to correct for the absorption of the gamma ray in the foil. For practical application, these are the desired correction factors; the gamma-ray absorption correction is required only for comparison with theory.

To facilitate interpolation, these correction factors were fitted with polynomials

$$\psi/\psi_o = \left(\sum_{i=0}^{n} a_i t^i \right)^{-1} ,$$

where ψ/ψ_o represents the correction factor and t is the foil thickness in mils. The coefficients and other pertinent data are given in Table A.17.

Table A.1. Experimentally Determined Activation per Unit Mass (ψ) of Thin 1-cm-Square Gold Foils in an Isotropic Flux

Mass (g)	ψ	$\sigma(\psi)$	Mass (g)	ψ	$\sigma(\psi)$
		Bare Foils			
3.9×10^{-5}	3.137×10^{9}	4.930×10^{7}	3.33×10^{-4}	2.679×10^{9}	3.814×10^{7}
4.0×10^{-5}	3.108×10^{9}	4.822×10^{7}	8.50×10^{-4}	2.458×10^{9}	3.504×10^{7}
4.9×10^{-5}	2.826×10^{9}	illegible	8.83×10^{-4}	2.561×10^{9}	4.074×10^{7}
6.6×10^{-5}	2.713×10^{9}	3.979×10^{7}	8.93×10^{-4}	2.357×10^{9}	3.364×10^{7}
7.1×10^{-5}	2.865×10^{9}	5.745×10^{7}	9.04×10^{-4}	2.472×10^{9}	4.953×10^{7}
8.78×10^{-5}	2.212×10^{9}	3.544×10^{7}	9.12×10^{-4}	2.681×10^{9}	4.266×10^{7}
8.9×10^{-5}	2.171×10^{9}	3.137×10^{7}	9.30×10^{-4}	2.770×10^{9}	5.885×10^{7}
2.13×10^{-4}	2.817×10^{9}	4.018×10^{7}	9.44×10^{-4}	2.783×10^{9}	5.577×10^{7}
2.18×10^{-4}	2.499×10^{9}	3.975×10^{7}	9.90×10^{-4}	2.551×10^{9}	5.422×10^{7}
2.18×10^{-4}	2.666×10^{9}	3.795×10^{7}	1.427×10^{-3}	2.596×10^{9}	3.704×10^{7}
2.31×10^{-4}	2.586×10^{9}	5.184×10^{7}	1.456×10^{-3}	2.444×10^{9}	3.905×10^{7}
2.52×10^{-4}	2.244×10^{9}	3.192×10^{7}	1.502×10^{-3}	2.502×10^{9}	3.565×10^{7}
2.52×10^{-4}	2.475×10^{9}	3.564×10^{7}	1.526×10^{-3}	2.461×10^{9}	3.916×10^{7}
2.90×10^{-4}	2.597×10^{9}	3.697×10^{7}	1.570×10^{-3}	2.561×10^{9}	5.135×10^{7}
		Cadmium-Covered Foils			
4.9×10^{-5}	7.922×10^{8}	1.499×10^{7}	3.33×10^{-4}	7.527×10^{8}	1.314×10^{7}
5.6×10^{-5}	6.893×10^{8}	1.207×10^{7}	8.01×10^{-4}	7.056×10^{8}	1.250×10^{7}
7.6×10^{-5}	6.838×10^{8}	1.543×10^{7}	8.36×10^{-4}	6.979×10^{8}	1.229×10^{7}
2.12×10^{-4}	9.500×10^{8}	1.662×10^{7}	1.000×10^{-3}	6.104×10^{8}	1.441×10^{7}
2.41×10^{-4}	7.076×10^{8}	1.677×10^{7}	1.050×10^{-3}	6.814×10^{8}	1.530×10^{7}
2.44×10^{-4}	6.905×10^{8}	1.552×10^{7}	1.650×10^{-3}	6.404×10^{8}	1.511×10^{7}
2.46×10^{-4}	7.268×10^{8}	1.269×10^{7}	1.682×10^{-3}	6.526×10^{8}	1.142×10^{7}

Table A.2. Experimentally Determined Activation per Unit Mass (ψ) of Thick 1-cm-Square Gold Foils in an Isotropic Flux

Mass (g)	ψ	$\sigma(\psi)$	Mass (g)	ψ	$\sigma(\psi)$
		Bare Foils			
2.7×10^{-3}	2.375×10^{9}	5.191×10^{7}	1.543×10^{-1}	1.699×10^{9}	3.400×10^{7}
1.11×10^{-2}	2.363×10^{9}	5.130×10^{7}	1.928×10^{-1}	1.683×10^{9}	3.898×10^{7}
1.135×10^{-2}	2.214×10^{9}	3.667×10^{7}	2.325×10^{-1}	1.585×10^{9}	2.521×10^{7}
2.36×10^{-2}	2.228×10^{9}	4.483×10^{7}	2.365×10^{-1}	1.577×10^{9}	2.508×10^{7}
2.42×10^{-2}	2.134×10^{9}	3.060×10^{7}	2.372×10^{-1}	1.578×10^{9}	3.159×10^{7}
4.70×10^{-2}	2.040×10^{9}	3.319×10^{7}	3.285×10^{-1}	1.402×10^{9}	2.569×10^{7}
4.70×10^{-2}	2.036×10^{9}	4.084×10^{7}	3.331×10^{-1}	1.426×10^{9}	2.266×10^{7}
7.52×10^{-2}	2.015×10^{9}	4.039×10^{7}	3.354×10^{-1}	1.444×10^{9}	2.891×10^{7}
8.20×10^{-2}	1.865×10^{9}	2.968×10^{7}	3.752×10^{-1}	1.390×10^{9}	2.782×10^{7}
8.68×10^{-2}	1.928×10^{9}	4.099×10^{7}	3.792×10^{-1}	1.377×10^{9}	2.189×10^{7}
1.012×10^{-1}	1.817×10^{9}	2.892×10^{7}	3.857×10^{-1}	1.359×10^{9}	2.160×10^{7}
1.227×10^{-1}	1.811×10^{9}	3.848×10^{7}	4.827×10^{-1}	1.248×10^{9}	2.498×10^{7}
1.235×10^{-1}	1.919×10^{9}	3.711×10^{7}	4.911×10^{-1}	1.241×10^{9}	1.973×10^{7}
1.485×10^{-1}	1.777×10^{9}	2.825×10^{7}	4.925×10^{-1}	1.226×10^{9}	1.950×10^{7}
1.517×10^{-1}	1.628×10^{9}	2.589×10^{7}			
		Cadmium-Covered Foils			
1.13×10^{-2}	4.882×10^{8}	1.114×10^{7}	1.543×10^{-1}	1.774×10^{8}	3.085×10^{6}
2.365×10^{-2}	3.830×10^{8}	6.703×10^{6}	1.928×10^{-1}	1.592×10^{8}	2.768×10^{6}
2.41×10^{-2}	3.729×10^{8}	8.407×10^{6}	1.933×10^{-1}	1.618×10^{8}	3.636×10^{6}
4.57×10^{-2}	2.986×10^{8}	5.202×10^{6}	2.284×10^{-1}	1.496×10^{8}	2.604×10^{6}
4.74×10^{-2}	2.977×10^{8}	6.696×10^{6}	2.331×10^{-1}	1.420×10^{8}	3.190×10^{6}
7.31×10^{-2}	2.505×10^{8}	5.634×10^{6}	3.354×10^{-1}	1.212×10^{8}	2.725×10^{6}
8.52×10^{-2}	2.284×10^{8}	3.973×10^{6}	3.368×10^{-1}	1.220×10^{8}	2.120×10^{6}
8.65×10^{-2}	2.354×10^{8}	5.291×10^{6}	3.746×10^{-1}	1.151×10^{8}	2.587×10^{6}
1.017×10^{-1}	2.128×10^{8}	3.701×10^{6}	3.902×10^{-1}	1.147×10^{8}	1.993×10^{6}
1.228×10^{-1}	1.778×10^{8}	4.182×10^{6}	4.798×10^{-1}	1.068×10^{8}	2.391×10^{6}
1.506×10^{-1}	1.772×10^{8}	3.985×10^{6}	4.827×10^{-1}	1.012×10^{8}	2.274×10^{6}

Table A.3. Experimentally Determined Activation per Unit Mass (ψ) of Disk-Shaped Gold Foils in an Isotropic Flux

Bare Foils			Cadmium-Covered Foils		
Mass (g)	ψ	$\sigma(\psi)$	Mass (g)	ψ	$\sigma(\psi)$
0.5-cm-dia Foils					
1.05×10^{-2}	2.092×10^{9}	5.454×10^{7}	1.06×10^{-2}	3.306×10^{8}	9.010×10^{6}
1.09×10^{-2}	2.115×10^{9}	5.509×10^{7}	1.10×10^{-2}	3.232×10^{8}	8.867×10^{6}
1.65×10^{-2}	2.005×10^{9}	5.178×10^{7}	1.64×10^{-2}	2.762×10^{8}	7.497×10^{6}
1.65×10^{-2}	2.023×10^{9}	4.664×10^{7}	1.64×10^{-2}	2.798×10^{8}	6.992×10^{6}
2.17×10^{-2}	1.975×10^{9}	5.101×10^{7}	2.16×10^{-2}	2.461×10^{8}	6.746×10^{6}
2.19×10^{-2}	1.952×10^{9}	5.042×10^{7}	2.19×10^{-2}	2.484×10^{8}	6.804×10^{6}
2.47×10^{-2}	1.940×10^{9}	4.994×10^{7}	2.49×10^{-2}	2.404×10^{8}	6.560×10^{6}
2.49×10^{-2}	1.929×10^{9}	4.976×10^{7}	2.52×10^{-2}	2.317×10^{8}	6.326×10^{6}
4.87×10^{-2}	1.760×10^{9}	4.523×10^{7}	4.87×10^{-2}	1.750×10^{8}	4.728×10^{6}
4.89×10^{-2}	1.760×10^{9}	4.524×10^{7}	4.89×10^{-2}	1.761×10^{8}	4.758×10^{6}
6.07×10^{-2}	1.672×10^{9}	4.303×10^{7}	6.07×10^{-2}	1.615×10^{8}	4.353×10^{6}
6.21×10^{-2}	1.674×10^{9}	4.308×10^{7}	6.20×10^{-2}	1.600×10^{8}	4.313×10^{6}
9.55×10^{-2}	1.514×10^{9}	3.891×10^{7}	9.49×10^{-2}	1.314×10^{8}	3.530×10^{6}
9.86×10^{-2}	1.502×10^{9}	3.860×10^{7}	9.81×10^{-2}	1.294×10^{8}	3.477×10^{6}
1-cm-dia Foils					
4.24×10^{-2}	2.026×10^{9}	4.639×10^{7}	4.34×10^{-2}	3.092×10^{8}	7.457×10^{6}
4.50×10^{-2}	1.985×10^{9}	5.113×10^{7}	4.48×10^{-2}	3.048×10^{8}	8.186×10^{6}
6.84×10^{-2}	1.893×10^{9}	4.867×10^{7}	6.85×10^{-2}	2.577×10^{8}	6.905×10^{6}

Table A.3. (cont.)

Bare Foils			Cadmium-Covered Foils		
Mass (g)	ψ	$\sigma(\psi)$	Mass (g)	ψ	$\sigma(\psi)$
1-cm-dia Foils (cont.)					
6.99×10^{-2}	1.912×10^{9}	4.373×10^{7}	7.01×10^{-2}	2.542×10^{8}	6.127×10^{6}
8.89×10^{-2}	1.849×10^{9}	4.749×10^{7}	8.90×10^{-2}	2.317×10^{8}	6.198×10^{6}
8.92×10^{-2}	1.831×10^{9}	4.325×10^{7}	8.93×10^{-2}	2.250×10^{8}	5.594×10^{6}
1.103×10^{-1}	1.781×10^{9}	4.573×10^{7}	1.104×10^{-1}	2.112×10^{8}	5.647×10^{6}
1.114×10^{-1}	1.781×10^{9}	4.076×10^{7}	1.121×10^{-1}	2.082×10^{8}	5.165×10^{6}
1.938×10^{-1}	1.587×10^{9}	3.745×10^{7}	1.947×10^{-1}	1.589×10^{8}	3.942×10^{6}
1.956×10^{-1}	1.577×10^{9}	4.046×10^{7}	1.958×10^{-1}	1.619×10^{8}	4.475×10^{6}
2.597×10^{-1}	1.469×10^{9}	3.466×10^{7}	2.617×10^{-1}	1.408×10^{8}	3.495×10^{6}
2.716×10^{-1}	1.453×10^{9}	3.726×10^{7}	2.714×10^{-1}	1.385×10^{8}	3.706×10^{6}
3.874×10^{-1}	1.290×10^{9}	2.827×10^{7}	3.887×10^{-1}	1.145×10^{8}	2.849×10^{6}
3.941×10^{-1}	1.288×10^{9}	3.302×10^{7}	3.935×10^{-1}	1.161×10^{8}	3.104×10^{6}
2-cm-dia Foils					
0.1542	2.077×10^{9}	5.350×10^{7}	0.1542	3.347×10^{8}	8.997×10^{6}
0.1542	2.016×10^{9}	4.508×10^{7}	0.1542	3.206×10^{8}	7.574×10^{6}
0.1542	2.005×10^{9}	4.738×10^{7}	0.1542	3.236×10^{8}	8.052×10^{6}
0.2560	1.890×10^{9}	4.462×10^{7}	0.2585	2.708×10^{8}	7.270×10^{6}
0.2579	1.936×10^{9}	4.976×10^{7}	0.2585	2.565×10^{8}	6.052×10^{6}
0.2579	1.878×10^{9}	4.433×10^{7}	0.2585	2.610×10^{8}	6.490×10^{6}

Table A.3. (cont.)

Bare Foils			Cadmium-Covered Foils		
Mass (g)	ψ	$\sigma(\psi)$	Mass (g)	ψ	$\sigma(\psi)$
		2-cm-dia Foils (cont.)			
0.3714	1.826×10^9	4.691×10^7	0.3714	2.233×10^8	5.543×10^6
0.3722	1.784×10^9	3.983×10^7	0.3715	2.293×10^8	6.153×10^6
0.3728	1.775×10^9	4.187×10^7	0.3728	2.200×10^8	5.187×10^6
0.4357	1.707×10^9	3.810×10^7	0.4444	2.044×10^8	4.821×10^6
0.4558	1.700×10^9	4.010×10^7	0.4686	2.063×10^8	5.532×10^6
0.4634	1.749×10^9	4.491×10^7	0.4686	2.024×10^8	5.030×10^6
0.7746	1.545×10^9	3.963×10^7	0.7787	1.630×10^8	4.373×10^6
0.7746	1.494×10^9	3.521×10^7	0.7787	1.602×10^8	3.975×10^6
0.7819	1.496×10^9	3.339×10^7	0.7863	1.582×10^8	3.729×10^6
1.0836	1.347×10^9	3.174×10^7	1.0836	1.458×10^8	3.905×10^6
1.0855	1.378×10^9	3.534×10^7	1.0964	1.338×10^8	3.155×10^6
1.0919	1.329×10^9	2.966×10^7	1.0964	1.358×10^8	3.372×10^6
1.5538	1.046×10^9	2.335×10^7	1.5551	1.115×10^8	2.628×10^6
1.5538	1.157×10^9	2.727×10^7	1.5570	1.167×10^8	3.125×10^6
1.5577	1.199×10^9	3.073×10^7	1.5577	1.138×10^8	2.823×10^6
		3-cm-dia Foils			
0.3355	2.070×10^9	5.313×10^7	0.3732	3.272×10^8	8.772×10^6
0.3355	2.001×10^9	4.468×10^7	0.3732	3.114×10^8	7.341×10^6
0.3355	2.011×10^9	4.746×10^7	0.3732	3.200×10^8	7.948×10^6

Table A.3. (cont.)

Bare Foils			Cadmium-Covered Foils		
Mass (g)	ψ	$\sigma(\psi)$	Mass (g)	ψ	$\sigma(\psi)$
3-cm-dia Foils (cont.)					
0.5866	1.861×10^9	4.389×10^7	0.8199	2.204×10^8	5.187×10^6
0.8112	1.710×10^9	3.816×10^7	0.8199	2.257×10^8	5.590×10^6
0.8112	1.717×10^9	4.048×10^7	0.8287	2.324×10^8	6.224×10^6
0.8258	1.786×10^9	4.581×10^7	1.0314	2.083×10^8	5.579×10^6
1.0246	1.693×10^9	4.340×10^7	1.0470	1.995×10^8	4.699×10^6
1.0314	1.633×10^9	3.643×10^7	1.1648	1.921×10^8	4.762×10^6
1.1203	1.614×10^9	3.806×10^7	1.8028	1.520×10^8	3.577×10^6
1.7941	1.378×10^9	3.075×10^7	1.8089	1.618×10^8	4.327×10^6
1.7941	1.394×10^9	3.285×10^7	1.8089	1.563×10^8	3.869×10^6
1.8028	1.507×10^9	3.938×10^7	2.4675	1.349×10^8	3.337×10^6
2.4445	1.231×10^9	2.901×10^7	2.4882	1.378×10^8	3.681×10^6
2.4977	1.265×10^9	3.241×10^7	2.5230	1.325×10^8	3.115×10^6
3.4942	1.073×10^9	2.750×10^7	3.5024	1.141×10^8	3.046×10^6
3.5024	1.008×10^9	2.249×10^7	3.5184	1.099×10^8	2.583×10^6
3.5024	1.026×10^9	2.417×10^7	3.5184	1.119×10^8	2.768×10^6

Table A.4. Experimentally Determined Activation per Unit Mass (ψ) of 1-cm-Square Gold Foils in an Anisotropic Flux with Relaxation Lenght λ = 5.8 cm

Mass (g)	ψ	$\sigma(\psi)$	Mass (g)	ψ	$\sigma(\psi)$
		Bare Foils			
1.05×10^{-3}	4.714×10^{6}	2.290×10^{5}	1.012×10^{-1}	3.953×10^{6}	6.578×10^{4}
1.23×10^{-3}	4.347×10^{6}	1.792×10^{5}	1.572×10^{-1}	3.839×10^{6}	6.233×10^{4}
1.125×10^{-2}	4.581×10^{6}	6.874×10^{4}	1.950×10^{-1}	3.556×10^{6}	5.143×10^{4}
2.45×10^{-2}	4.402×10^{6}	6.378×10^{4}	2.370×10^{-1}	3.399×10^{6}	4.971×10^{4}
4.68×10^{-2}	4.150×10^{6}	6.091×10^{4}	3.362×10^{-1}	3.116×10^{6}	4.508×10^{4}
7.85×10^{-2}	4.046×10^{6}	5.880×10^{4}	3.761×10^{-1}	3.012×10^{6}	4.346×10^{4}
1.006×10^{-1}	3.819×10^{6}	6.844×10^{4}	4.813×10^{-1}	2.839×10^{6}	4.608×10^{4}
		Cadmium-Covered Foils			
1.13×10^{-2}	5.018×10^{5}	9.742×10^{3}	1.958×10^{-1}	1.733×10^{5}	3.056×10^{3}
2.45×10^{-2}	3.797×10^{5}	6.927×10^{3}	2.359×10^{-1}	1.643×10^{5}	3.236×10^{3}
4.57×10^{-2}	3.140×10^{5}	5.765×10^{3}	3.362×10^{-1}	1.316×10^{5}	2.296×10^{3}
7.88×10^{-2}	2.525×10^{5}	4.537×10^{3}	3.776×10^{-1}	1.228×10^{5}	2.142×10^{3}
1.551×10^{-1}	1.930×10^{5}	3.444×10^{3}	4.776×10^{-1}	1.099×10^{5}	2.050×10^{3}

Table A.5. Parameters to Fit the Curve of the Activation per Unit Mass of Bare and Cadmium-Covered Thin 1-cm-Square Gold Foils in an Isotropic Flux

SSRM, Bare Foils: 31.297
SSRM, Cadmium-Covered Foils: 21.266

Foil	Coefficients	((V))	
Bare	$a_o = (2.544 \pm 0.043) \times 10^9$	5.955×10^{13}	
Cadmium-Covered	$a_o = (7.50 \pm 0.26) \times 10^8$	3.167×10^{13}	-2.785×10^{16}
	$a_1 = (-6.62 \pm 3.03) \times 10^{10}$	-2.785×10^{16}	4.316×10^{19}

Table A.6. Parameters to Fit the Curve of the Activation per Unit Mass of Bare and Cadmium-Covered Thick 1-cm-Square Gold Foils in an Isotropic Flux

Coefficients			((V))		
Bare Foils; SSRM = 2.049					
$a_0 \equiv 0$					
$a_1 = (1.956 \pm 0.063) \times 10^9$	1.922×10^{15}	2.478×10^6	-1.307×10^{15}	1.631×10^8	
$a_2 = 0.938 \pm 0.083$	2.478×10^5	3.377×10^{-3}	-1.741×10^6	2.020×10^{-1}	
$a_3 = (4.05 \pm 0.60) \times 10^8$	-1.307×10^{15}	-1.741×10^6	1.773×10^{15}	-6.805×10^7	
$a_4 = 17.6 \pm 6.1$	1.631×10^8	2.020×10^{-1}	-6.805×10^7	1.806×10^1	
Cadmium-Covered Foils; SSRM = 1.886					
$a_0 = (8.84 \pm 0.71) \times 10^7$	2.668×10^{13}	5.248×10^{13}	3.418×10^6	-3.262×10^{13}	1.582×10^7
$a_1 = (1.96 \pm 0.18) \times 10^8$	5.248×10^{13}	1.791×10^{14}	8.242×10^6	-5.048×10^{13}	5.462×10^7
$a_2 = 5.27 \pm 0.89$	3.418×10^6	8.242×10^6	4.726×10^{-1}	-4.154×10^6	2.452×10^0
$a_3 = (2.96 \pm 0.25) \times 10^8$	-3.262×10^{13}	-5.048×10^{13}	-4.154×10^6	3.404×10^{14}	1.400×10^7
$a_4 = 35.7 \pm 6.2$	1.582×10^7	5.462×10^7	2.452×10^0	1.400×10^7	2.052×10^1

Table A.7. Parameters to Fit the Curve of the Activation per Unit Mass of Bare and Cadmium-Covered 0.5-cm-dia Gold Foils in an Isotropic Flux

Coefficients	((V))			
Bare Foils; SSRM = 0.0496				
$a_0 \equiv 0$				
$a_1 = (2.00 \pm 0.21) \times 10^9$	4.491×10^{16}	2.358×10^8	-1.653×10^{16}	1.546×10^{10}
$a_2 = 2.91 \pm 1.13$	2.358×10^8	1.269×10^0	-9.747×10^7	7.834×10^1
$a_3 = (2.95 \pm 1.58) \times 10^8$	-1.663×10^{16}	-9.747×10^7	2.505×10^{16}	-1.974×10^9
$a_4 = 55.5 \pm 78.6$	1.546×10^{10}	7.834×10^1	-1.974×10^9	6.174×10^3
Cadmium-Covered Foils; SSRM = 0.1545				
$a_0 \equiv 0$				
$a_1 = (2.20 \pm 0.17) \times 10^8$	2.897×10^{14}	1.499×10^7	1.112×10^{14}	2.049×10^8
$a_2 = 5.46 \pm 0.90$	1.499×10^7	8.053×10^{-1}	4.107×10^6	1.010×10^1
$a_3 = (2.62 \pm 0.29) \times 10^8$	1.112×10^{14}	4.107×10^6	8.655×10^{14}	2.615×10^8
$a_4 = 73.8 \pm 13.8$	2.049×10^8	1.010×10^1	2.615×10	1.906×10^2

Table A.8. Parameters to Fit the Curve of the Activation per Unit Mass of Bare and Cadmium-Covered 1.0-cm-dia Gold Foils in an Isotropic Flux

Coefficients		((V))		
Bare Foils; SSRM = 0.0476				
$a_o \equiv 0$				
$a_1 = (1.83 \pm 0.37) \times 10^9$	1.401×10^{17}	1.740×10^8	-1.001×10^{17}	4.940×10^9
$a_2 = (9.12 \pm 4.67) \times 10^{-1}$	1.740×10^8	2.183×10^{-1}	-1.265×10^8	6.022×10^0
$a_3 = (3.89 \pm 2.82) \times 10^8$	-1.001×10^{17}	-1.265×10^8	7.969×10^{16}	-3.247×10^9
$a_4 = 10.5 \pm 13.6$	4.940×10^9	6.022×10^0	-3.247×10^9	1.856×10^2
Cadmium-Covered Foils; SSRM = 0.1892				
$a_o \equiv 0$				
$a_1 = (2.03 \pm 0.16) \times 10^8$	2.651×10^{14}	3.655×10^6	7.623×10^{13}	4.495×10^7
$a_2 = 1.44 \pm 0.23$	3.655×10^6	5.196×10^{-2}	7.371×10^5	5.955×10^{-1}
$a_3 = (2.56 \pm 0.25) \times 10^8$	7.623×10^{13}	7.371×10^5	6.121×10^{14}	4.508×10^7
$a_4 = 17.97 \pm 3.10$	4.495×10^7	5.955×10^{-1}	4.508×10^7	9.622×10^0

Table A.9. Parameters to Fit the Curve of the Activation per Unit Mass of Bare and Cadmium-Covered 2.0-cm-dia Gold Foils in an Isotropic Flux

Coefficients	((V))			
Bare Foils; SSRM = 1.470				
$a_o \equiv 0$				
$a_1 = (2.032 \pm .079) \times 10^9$	4.249×10^{15}	1.659×10^6	9.728×10^{15}	3.695×10^8
$a_2 = 0.382 \pm .032$	1.659×10^6	6.937×10^{-4}	3.472×10^6	1.378×10^{-1}
$a_3 = (3.46 \pm 3.29) \times 10^8$	9.728×10^{15}	3.472×10^6	7.373×10^{16}	1.567×10^9
$a_4 = 7.18 \pm 7.99$	3.695×10^8	1.378×10^{-1}	1.567×10^9	4.346×10^1
Cadmium-Covered Foils; SSRM = 0.8437				
$a_o \equiv 0$				
$a_1 = (2.149 \pm 0.109) \times 10^8$	1.181×10^{14}	4.044×10^5	6.205×10^{13}	6.118×10^6
$a_2 = 0.411 \pm .038$	4.044×10^5	1.440×10^{-3}	1.740×10^5	2.013×10^{-2}
$a_3 = (2.75 \pm 0.21) \times 10^8$	6.205×10^{13}	1.740×10^5	4.430×10^{14}	8.932×10^6
$a_4 = 5.24 \pm 0.64$	6.118×10^6	2.013×10^{-2}	8.932×10^6	4.110×10^{-1}

Table A.10. Parameters to Fit the Curve of the Activation per Unit Mass of Bare and Cadmium-Covered 3.0-cm-dia Gold Foils in an Isotropic Flux

Coefficients			((V))	
Bare Foils; SSRM = 1.178				
$a_o \equiv 0$				
$a_1 = (1.965 \pm .084) \times 10^9$	6.022×10^{15}	1.030×10^6	6.764×10^{15}	1.266×10^8
$a_2 = 0.184 \pm .015$	1.030×10^6	1.865×10^{-4}	1.030×10^6	2.076×10^{-2}
$a_3 = (4.46 \pm 2.04) \times 10^8$	6.764×10^{15}	1.030×10^6	3.526×10^{16}	2.738×10^8
$a_4 = 2.76 \pm 2.00$	1.266×10^8	2.076×10^{-2}	2.738×10^8	3.396×10^0
Cadmium-Covered Foils; SSRM = 0.7777				
$a_o \equiv 0$				
$a_1 = (2.07 \pm 0.12) \times 10^8$	1.502×10^{14}	2.300×10^5	6.008×10^{13}	3.080×10^6
$a_2 = 0.176 \pm 0.019$	2.300×10^5	3.632×10^{-4}	7.317×10^4	4.545×10^{-3}
$a_3 = (2.78 \pm 0.21) \times 10^8$	6.008×10^{13}	7.317×10^4	4.256×10^{14}	3.505×10^6
$a_4 = 2.16 \pm 0.28$	3.080×10^6	4.545×10^{-3}	3.505×10^6	7.909×10^{-2}

Table A.11. Parameters to Fit the Curve of the Activation per Unit Mass of Bare and Cadmium-Covered 1-cm-Square Gold Foils in an Anisotropic Flux with Relaxation Length $\lambda = 5.8$ cm

Coefficients	((V))				
Bare Foils; SSRM = 1.579					
$a_o \equiv 0$					
$a_1 = (4.14 \pm 0.15) \times 10^6$	2.352×10^{10}	1.465×10^4	-1.347×10^{10}	1.231×10^6	
$a_2 = 0.819 \pm 0.098$	1.465×10^4	9.555×10^{-3}	-1.176×10^4	7.367×10^{-1}	
$a_3 = (4.83 \pm 1.39) \times 10^5$	-1.847×10^{10}	-1.176×10^4	1.937×10^{10}	-7.756×10^5	
$a_4 = 15.2 \pm 8.9$	1.231×10^6	7.367×10^{-1}	-7.756×10^5	7.929×10^1	
Cadmium-Covered Foils; SSRM = 1.502					
$a_o = (9.14 \pm 0.61) \times 10^4$	3.689×10^7	4.423×10^7	3.502×10^3	2.939×10^6	3.164×10^4
$a_1 = (2.39 \pm 0.12) \times 10^5$	4.423×10^7	1.516×10^8	5.877×10^3	6.386×10^7	9.039×10^4
$a_2 = 5.34 \pm 0.61$	3.502×10^3	5.877×10^3	3.671×10^{-1}	1.053×10^3	3.836×10^0
$a_3 = (3.34 \pm 0.32) \times 10^5$	2.939×10^6	6.386×10^7	1.053×10^3	1.011×10^9	1.700×10^5
$a_4 = 54.7 \pm 8.9$	3.164×10^4	9.039×10^4	3.836×10^0	1.700×10^5	7.917×10^1

Table A.12. Experimentally Determined Flux Depression Corrections for Gold Foils Exposed in an Isotropic Flux in Water

Foil Thickness (mil)	1-cm-Square Foil	0.5-cm-dia Foil	1-cm-dia Foil	2-cm-dia Foil	3-cm-dia Foil
0.5	0.997 ± 0.031				
1.0	0.974 ± 0.030	0.990 ± 0.036	0.951 ± 0.035	0.930 ± 0.033	0.940 ± 0.031
1.5		0.977 ± 0.030	0.932 ± 0.029	0.919 ± 0.029	0.898 ± 0.028
2.0	0.915 ± 0.027	0.963 ± 0.029	0.911 ± 0.027	0.892 ± 0.028	0.863 ± 0.027
3.0	0.866 ± 0.026	0.934 ± 0.030	0.869 ± 0.027	0.843 ± 0.025	0.805 ± 0.024
4.0	0.826 ± 0.025				
5.0	0.790 ± 0.024	0.880 ± 0.028	0.795 ± 0.025	0.754 ± 0.024	0.709 ± 0.022
7.0	0.723 ± 0.022	0.833 ± 0.026	0.733 ± 0.023	0.673 ± 0.020	0.624 ± 0.019
8.0	0.692 ± 0.021				
10.0	0.631 ± 0.020	0.769 ± 0.026	0.657 ± 0.022	0.565 ± 0.019	0.515 ± 0.017

Table A.13. Parameters to Fit the Curve of the Experimentally Determined Flux Depression Correction Factors for Gold Foils in an Isotropic Flux

Coefficients	((v))		
1-cm-Square Foils, SSRM = 2.727×10^{-2}			
$a_o = 0.970 \pm 0.020$	3.877×10^{-4}	-6.607×10^{-5}	
$a_1 = (6.01 \pm 0.43) \times 10^{-2}$	-6.607×10^{-5}	1.814×10^{-5}	
0.5-cm-dia Foils, SSRM = 2.039×10^{-3}			
$a_o = 0.975 \pm 0.022$	4.973×10^{-4}	-8.628×10^{-5}	
$a_1 = (3.24 \pm 0.48) \times 10^{-2}$	-8.628×10^{-5}	2.337×10^{-5}	
1-cm-dia Foils, SSRM = 3.738×10^{-3}			
$a_o = 0.994 \pm 0.024$	5.568×10^{-4}	-1.004×10^{-4}	
$a_1 = (5.27 \pm 0.53) \times 10^{-2}$	-1.004×10^{-4}	2.854×10^{-5}	
2-cm-dia Foils, SSRM = 1.166×10^{-2}			
$a_o = 1.001 \pm 0.042$	1.789×10^{-3}	-8.796×10^{-4}	7.734×10^{-5}
$a_1 = (5.41 \pm 2.29) \times 10^{-2}$	-8.796×10^{-4}	5.255×10^{-4}	-4.955×10^{-5}
$a_2 = (2.25 \pm 2.23) \times 10^{-3}$	7.734×10^{-5}	-4.955×10^{-5}	4.990×10^{-6}
3-cm-dia Foils, SSRM = 4.489×10^{-2}			
$a_o = 0.996 \pm 0.043$	1.854×10^{-3}	-9.303×10^{-4}	8.236×10^{-5}
$a_1 = (7.37 \pm 2.38) \times 10^{-2}$	-9.303×10^{-4}	5.679×10^{-4}	-5.389×10^{-5}
$a_2 = (2.00 \pm 2.34) \times 10^{-3}$	8.236×10^{-5}	-5.389×10^{-5}	5.470×10^{-6}

Table A.14. Parameters to Fit the Curve of the Experimentally Determined Flux Depression Correction Factors for 1-cm-Square Gold Foils in an Anisotropic Flux with Relaxation Length λ = 5.8 cm

SSRM = 2.831×10^{-3}

Coefficients	((V))	
$a_o = 0.965 \pm 0.043$	1.833×10^{-3}	-3.082×10^{-4}
$a_1 = (5.15 \pm 0.91) \times 10^{-2}$	-3.082×10^{-4}	8.309×10^{-5}

THIS PAGE

WAS INTENTIONALLY

LEFT BLANK

ORNL-3407
UC-34 — Physics
TID-4500 (19th ed.)

INTERNAL DISTRIBUTION

1. Biology Library
2-3. Central Research Library
4. Reactor Division Library
5-6. ORNL — Y-12 Technical Library Document Reference Section
7-56. Laboratory Records Department
57. Laboratory Records, ORNL R.C.
58. T. D. Anderson
59. E. D. Arnold
60. J. A. Auxier
61. E. P. Blizard
62. J. S. Cheka
63. R. D. Cheverton
64. H. C. Claiborne
65. C. E. Clifford
66. F. J. Davis
67. F. F. Dyer
68. R. L. Ferguson
69. G. Goldstein
70. J. Halperin
71. W. H. Jordan
72. C. E. Larson
73. D. W. Magnuson
74-83. F. C. Maienschein
84. J. T. Mihalczo
85. A. M. Perry
86. G. W. Peterson
87. J. J. Pinajian
88. C. A. Preskitt
89. P. W. Reinhardt
90. S. A. Reynolds
91. R. H. Ritchie
92. F. W. Sanders
93. M. J. Skinner
94. J. E. Strain
95. J. A. Swartout
96. J. H. Thorngate
97. D. K. Trubey
98. C. D. Zerby
99-124. W. Zobel
125. R. A. Charpie (consultant)
126. P. F. Cast (consultant)
127. R. F. Taschek (consultant)
128. T. J. Thompson (consultant)

EXTERNAL DISTRIBUTION

129. Robert C. Doerner, Reactor Engineering Division, Argonne National Laboratory, 9700 South Cass Avenue, Argonne, Illinois
130. G. Ronald Dalton, Department of Nuclear Engineering, University of Florida, Gainesville, Florida
131. C. W. Tittle, School of Engineering, Southern Methodist University, Dallas 22, Texas
132. James H. Roberts, Physics Department, Northwestern University, Evanston, Illinois
133. E. D. Klema, Northwestern University, The Technological Institute, Evanston, Illinois
134. Richard K. Osborn, Professor of Nuclear Engineering, University of Michigan, Ann Arbor, Michigan
135. Randall S. Caswell, National Bureau of Standards, Neutron Physics Section, Washington 25, D.C.
136. B. C. Diven, Los Alamos Scientific Laboratory, Los Alamos, New Mexico
137. F. R. Nakache, United Nuclear Corporation, 5 New Street, White Plains, New York
138. Herbert Goldstein, United Nuclear Corporation, 5 New Street, White Plains, New York
139. Research and Development Division, AEC, ORO
140-701. Given distribution as shown in TID-4500 (19th ed.) under Physics category